Title page

Title: A library of lineage-specific driver lines connects developing neuronal circuits to behavior in the *Drosophila* Ventral Nerve Cord.

Authors:
Jelly HM Soffers[1]*, Erin Beck[1], Daniel J. Sytkowski[1], Marianne E. Maughan[1], Devasri Devarakonda[1], Yi Zhu[2], Beth Wilson[2], Yu-Chieh David Chen[3], Ted Erclik[4,5], James W. Truman[6], James B. Skeath[2], Haluk Lacin [1]*

Affiliations:
1: School of Science and Engineering, Division Biological and Biomedical Systems, University of Missouri-Kansas City, Kansas City, MO, USA.
2: Department of Genetics, Washington University School of Medicine, St. Louis, MO, USA,
3: Department of Biology, New York University, New York, NY, USA.
4: Department of Biology, University of Toronto - Mississauga, Mississauga, ON, Canada.
5: Department of Cell and Systems Biology, University of Toronto - Mississauga, Mississauga, ON, Canada.
6: Department of Biology, University of Washington, Seattle, WA, USA.
*: Corresponding authors: j.soffers@umkc.edu, hlhyr@umkc.edu

Abstract

Understanding developmental changes in neuronal lineages is crucial to elucidate how they assemble into functional neural networks. Studies investigating nervous system development in model systems have only focused on select regions of the central nervous system due to the limited availability of genetic drivers that target specific neuronal lineages throughout development and adult life. This has hindered our understanding of how distinct neuronal lineages interconnect to form neuronal circuits during development. Here, we present a split-GAL4 library composed of genetic driver lines, which we generated via editing the genomic locus of lineage-specific transcription factors and demonstrate that we can use this library to specifically target most individual neuronal hemilineages in the *Drosophila* ventral nerve cord (VNC) throughout development and into adulthood. Using these genetic driver lines, we found striking morphological changes in neuronal processes within a lineage during metamorphosis. We also demonstrated how neurochemical features of neuronal classes can be quickly assessed. Lastly, we documented

behaviors elicited in response to optogenetic activation of individual neuronal lineages and generated a comprehensive lineage-behavior map of the entire fly VNC. Looking forward, this lineage-specific split-GAL4 driver library will provide the genetic tools needed to address the questions emerging from the analysis of the recent VNC connectome and transcriptome datasets.

Introduction

Neuronal circuits underlie nervous system functions ranging from perception and movement to cognition and emotion. Most neurons found in the adult central nervous system (CNS) of animals are generated and assembled into circuits during development. Investigating the formation of these circuits provides valuable insights into the functional organization and operation of the nervous system, both in health and disease.

Drosophila has served as a powerful model system to investigate how neuronal circuits function due to its medium complexity compared to vertebrate models yet rich repertoire of behaviors, and unprecedented genetic toolkit. High-resolution electron microscopy data of the adult fly brain and ventral nerve cord (VNC) reveal individual neuronal morphologies and their synaptic connections (1-5). The integration of these morphological data with single-cell transcriptome profiles has placed the adult fly CNS at the forefront of studies of circuit operations at the molecular level (6-9).

In *Drosophila* and other model systems, less attention has been paid to how neuronal circuits develop compared to how they function, limiting our understanding of the developmental processes that instruct newly born neurons to assemble into functional circuits. In *Drosophila*, the same set of neural stem cells, called neuroblasts (NB), sequentially form the larval and adult CNS, with the adult CNS having 10 to 20-fold more neurons and a greater complexity. Some of the embryonic-born neurons, which function in the larval CNS, are remodeled to integrate into adult circuits (10-12). Most of the adult neurons are born post-embryonically during larval and early pupal stages. These neurons fully differentiate and assemble into circuits during metamorphosis into the adult, which lasts several days. This extended window of neurogenesis and neuronal maturation during the formation of the adult VNC facilitates experimental manipulations that are not feasible during the brief period of neurogenesis in the embryo, such as temporal gene silencing studies to discriminate axon guidance and synapse formation.

The fly VNC, like its vertebrate analog, the spinal cord, is functionally compartmentalized into lineally related groups of neurons, called neuronal lineages. In flies, Notch-mediated asymmetric cell division divides the neuronal population of each NB into two subclasses, called hemilineages: “A” hemilineages are composed of Notch ON cells and “B” hemilineages are composed of notch OFF cells (13-15). The adult fly VNC is composed of ~15,000 neurons, most of which are found

in the three thoracic segments. Each thoracic hemisegment contains 34 major post-embryonic hemilineages, with some segment-specific variation in the type of hemilineages and their morphology. Recent studies identified these hemilineages in the VNC Electron Microscopy (EM) volume dataset and showed that neurons within a given hemilineage exhibit a stereotyped pattern of connectivity (1, 2, 16, 17). This revealed that hemilineages display a propensity to form synaptic connections with neurons from other specific hemilineages, uncovering a macro-connectivity among hemilineages. Hemilineage-based compartmentalization of the VNC is also observed at the level of gene expression. Allen *et al.,* (6) assessed the transcriptome of the entire adult VNC via single-cell RNA sequencing (scRNAseq) and showed that hemilineage identity correlates highly with unique clusters of cells, which are partitioned solely based on gene expression via dimensionality reduction. Lastly, several studies employing hemilineage-restricted neuronal manipulations showed that the VNC hemilineages represent functional modules that control animal behavior (18-20). Indeed, like the cardinal classes of interneurons in the spinal cord (21-23), hemilineages in the *Drosophila* VNC are functional units, each contributing to aspects that control specific behaviors. Thus, taking a hemilineage-based approach is essential for a systematic and comprehensive understanding of behavioral circuit assembly during development in complex nervous systems.

Addressing the question of how neurons in individual hemilineages develop into functional circuits requires genetic tools to manipulate individual hemilineages throughout development. Existing genetic driver lines (GAL4, Split-GAL4, and LexA libraries) are often limited in their use for developmental studies. The expression of such drivers typically relies on 2–3 kb genomic fragments that contain enhancer elements, (24)and comprehensive screening efforts have identified driver lines that mark specific neuronal populations ((24) and citations therein). However, the genomic fragments driving GAL4, Split-GAL4 or LexA expression lack the complete endogenous transcriptional control mechanisms. As a result, they are oftentimes only expressed in specific neuronal populations during particular life stages, such as exclusively in the larva or adult. Consequently, they lack the temporal stability required for comprehensive developmental analysis (24-26), highlighting a critical need for developmentally stable and hemilineage specific driver lines. These tools will allow us to track and measure individual hemilineages as well as activate or inactivate specific genes and neuronal functions within them, thereby facilitating the identification of fundamental principles underlying circuit development.

Here, we describe a split-GAL4 library that targets unique hemilineages in a developmentally stable manner. Our previous work demonstrated that many of the lineage-specific transcription factors that regulate the specification and differentiation of post-embryonic neurons are stably expressed during development (27-30). We employed gene knock-in strategies to insert split-GAL4 driver coding sequences in frame with the coding regions of these transcription factors, generating lineage-specific, temporally stable driver lines for selected hemilineages (20, 27, 28). To extend this approach to all hemilineages in the VNC, we required a more comprehensive list of lineage-specific transcription factors. To compile this list, we utilized published scRNA-seq data of the VNC and expanded upon the work of Allan et al. (27)(6). (19)This work had assigned a part of the scRNAseq cell clusters to hemilineages. We analyzed the gene expression patterns of the remaining clusters for combinations of significantly enriched transcription factors, referred to as cluster markers, and tested the expression patterns of these genes with genetic reporter lines and antibody staining. We were able to assign 33 of the 34 major hemilineages to scRNAseq clusters with this approach. Then, we generated gene-specific split-GAL4 lines for 28 of these hemilineage-specific transcription factors via genome editing and recombination techniques. We performed a thorough analysis of the expression patterns of binary combinations of split-GAL4 AD and split-GAL4 DBD lines using combinations of the 28 transcription factor-specific hemidrivers we present in this study and split-GAL4 lines generated previously (28, 30, 31). We report 44 combinations that target 32 of the 34 VNC hemilineages; most of these drivers do this specifically and in a developmentally stable manner. Finally, we demonstrate the ability of this library to map neurotransmitter expression to individual hemilineages and to map specific behaviors to defined neuronal lineages.

Results

Intersecting the expression of *acj6* and *unc-4* with the split-GAL4 method faithfully marks hemilineage 23B throughout development and adult life.

Many transcription factors in the CNS are expressed in a hemilineage specific manner, and their expression is generally maintained throughout the lifetime of the neurons that express them (27). We asked whether we could generate specific and temporally stable driver lines by hijacking the expression of such transcription factors. We initially focused on Acj6 and Unc-4, which are transcription factors expressed in numerous neuronal cell clusters in the brain and VNC (Figure 1A-B). Our prior work demonstrated that these proteins are co-expressed exclusively in hemilineage 23B neurons in both the larva and adult (27). We leveraged this unique co-expression pattern to develop a genetic set-up that targets only the 23B neurons in a developmentally stable manner. We combined two techniques: the Trojan-exon-based driver for target gene transcription (32) and the split-GAL4 method (33). The split-GAL4 method works by reconstituting GAL4 function through the interaction of GAL4's DNA-binding domain (DBD) and an activation domain (AD) in cells where both transgenes are expressed. Here we used the *unc-4* split-GAL4 AD and DBD lines that we had previously generated (20) and created *acj6* split-GAL4 lines by replacing the MIMIC insertion in the *acj6* coding intron with a Trojan exon encoding either p65.AD or GAL4-DBD via recombinase-mediated cassette exchange (RMCE).

By combining *unc-4*-GAL4^{AD} and *acj6*-GAL4^{DBD} transgenes in the same animal with a nuclear expression reporter gene, UAS-nls-tdTomato, we specifically visualized the thoracic clusters of 23B neurons in the adult CNS (Figure 1C). Small clusters of neurons were evident in the suboesophageal zone, and their projections suggest that they are the labial homologs of hemilineage 23B (Figure 1 - figure supplement-1D, E). Membranous GFP expression (UAS-myr-GFP) also highlighted axonal projections of a few leg, gustatory and antennal sensory neurons which are missed with nuclear-based methods such as immunostaining for nuclear transcription factors or nuclear GFP reporter genes, since sensory cell bodies are located outside of the CNS. The reverse combination (*unc-4*-GAL4^{DBD} and *acj6*-GAL4^{AD}) exhibited an almost identical expression pattern (not shown).

To verify that these gene-specific split-GAL4 drivers recapitulate the intersected expression patterns of *unc-4* and *acj6*, we performed immunostaining with antibodies against Acj6 and Unc-4 on embryos carrying the described transgenes and evaluated the overlap with the GFP signal.

Robust GFP expression was observed in the late-stage embryo and marked segmentally repeated clusters of neurons in the VNC (Figure 1 - figure supplement-1A, B). All GFP-positive cells were also positive for Acj6 and Unc-4 immunostaining, indicating that these cells correspond to the embryonic progeny of NB7-4, embryonic 23B neurons (20). Occasionally, one-to-two cells per segment expressed both transcription factors but not GFP (not shown). These cells, located ventrally, are likely late-born, immature neurons and their GFP expression may lag endogenous gene expression of Acj6 and Unc-4 due to the additional round of transcription and translation required for GFP expression. Outside the CNS, GFP-positive sensory neurons were found in the embryonic head region, where taste organs are located (not shown). Overall, the embryonic expression analysis confirmed that the *acj6*-GAL4^{DBD} and *unc-4*-GAL4^{AD} split-GAL4 combination accurately recapitulates co-expression of Acj6 and Unc-4 proteins and target embryonic 23B neurons. To test whether this combination of split-GAL4 driver lines also specifically marks 23B hemilineage during larval, pupal, and adult life, we carried out similar analysis during these stages. Like in the embryo, the intersection of *acj6*-GAL4^{DBD} and *unc-4*-GAL4^{AD} specifically marked 23B neurons in the larva, pupa, and adult (Figure 1 - figure supplement-1C, D). Thus, this split-GAL4 combination effectively targets reporter expression specifically to the 23B neurons in the VNC from the early larva through to the adult.

Identifying new marker genes for hemilineages and assigning hemilineages to scRNAseq clusters of the VNC transcriptome.

The example described above demonstrated that combining the Trojan exon method with the split-GAL4 approach holds the potential to generate temporally stable, lineage-specific driver lines for every hemilineage in the VNC, provided suitable pairs of genes are identified. Our prior work created a map of the expression of 20 transcription factors, each of which is expressed from early larval stages to the adult in most or all neurons of a small number of hemilineages in the adult VNC (20, 27, 28). When overlapped in a binary manner with each other, these transcription factors uniquely identify more than half of the 34 adult VNC hemilineages, rendering them ideal genomic targets from which to create a library of split-GAL4 driver lines.

To identify unique binary gene combinations that can selectively label each of the remaining hemilineages we further analyzed scRNAseq data from the adult VNC (6). Allen *et al.* defined 120 t-SNE clusters based on unique combinations of significantly enriched genes, referred to as cluster markers. By comparing these cluster markers to established lineage markers, the Goodwin group assigned 18 hemilineages to one or more clusters, leaving 16 hemilineages unassigned.

For example, they assigned grouped clusters 67, 93, 35 and 51 to lineage 23B. In agreement with our immunostaining that revealed that cluster markers *acj6* and *unc-4* mark this hemilineage (Figure 1C, D), we report that also the expression patterns of *acj6* and *unc-4* expression overlap in this grouped scRNAseq cluster (Figure 1E). We continued this approach and tested whether other cluster-specific marker genes were expressed in their corresponding hemilineages. For instance, Allen *et al.,* assigned clusters 0 and 100 to hemilineage 4B. Both clusters express *fkh, HLH4C*, and *oc* genes in addition to three additional genes: *hb9 (*also known as *exex), HGTX*, and *ap* which we had previously shown to be expressed in 4B neurons (34). Using GFP-tagged BAC reporter lines for *fkh*, *oc*, and *HLH4C* combined with immunostaining for Hb9 we demonstrate that cluster markers *fkh*, *oc and HLH4C* are indeed expressed in 4B neurons in the larval and adult VNC, consistent with the scRNAseq data (Figure 2A, data not shown). In addition to hemilineage 4B, Hb9 marks hemilineage 10B and 16B neurons (35). Hemilineage 10B was assigned to clusters 39, 68, and 91 and hemilineage 16B to clusters 5 and 46 (6). Knot (Kn) is a marker for clusters 39 and 91, and Sp1 for clusters 5 and 46. Reporters for both genes show that Kn and Sp1 are expressed in lineage 10B and 16B neurons, respectively (Figure 2B, C). Therefore, when a cluster marker, or marker combination, is uniquely associated with a hemilineage, it accurately marks this hemilineage.

To identify the clusters that correspond to the remaining 16 hemilineages not assigned by Allen *et al.,* we focused on the orphan clusters, which have not been assigned to any hemilineage. For each of these orphan clusters, we visualized the expression pattern of the cluster marker with reporter genes or antibody staining and studied the morphology of the neurons that expressed this cluster marker. To identify which hemilineage these neurons belonged to, we compared the observed morphology to the documented morphologies of unannotated hemilineages that used the same neurotransmitter as was expressed in the scRNAseq cluster. For example, glutamatergic clusters 15 and 86, which are adjacent in the t-SNE plot, are the only glutamatergic clusters that express Sox21a. To map these clusters to a hemilineage, we studied the morphology of the Sox21a-positive neurons in the VNC by expressing membrane-bound GFP under the control of a CRIMIC line reporting Sox21a expression (Figure 2D). This marked a group of ventral and anterior Sox21a-positive neuronal cell bodies situated near the midline in each hemisegment of the larval and adult VNC (Figure 2D). Their processes project dorsally and then sharply turn upon reaching the dorsal surface of the neuropil. Based on their glutamatergic neurotransmitter identity and their unique morphology, which matches that of 2A interneurons (19, 36), we assigned these clusters to hemilineage 2A.

Another example is cluster 58, which, among all the VNC hemilineages, uniquely co-expresses *unc-4* and *islet* (also known as tup) (27). We had previously studied Unc-4-positive hemilineages and had identified that hemilineage 17A is the only Unc-4-positive lineage that expresses Islet (20). To verify that cluster 58 identified hemilineage 17A neurons, we examined the expression pattern of another transcription factor, Hmx, which is a cluster marker for cluster 58 (6) Visualization of Hmx-positive neurons with a CRIMIC line reporting *Hmx* expression revealed that their cell bodies are located on the dorsal surface of the VNC and their processes project into the ipsilateral ventromedial neuropil, and then loop dorsally (Figure 2E). This morphology is typical of 17A neurons. Additionally, we found that cluster 77 is marked with the combination of *Hmx* and *tup* and is directly adjacent to cluster 58 in the adult VNC t-SNE plot (6). Thus, neurons of *Hmx*-positive clusters 58 and 77 likely belong to lineage 17A (Figure 2E). Furthermore, we noted that some transcription factors are expressed in a subset of neurons within a hemilineage and appeared to correspond to one of the multiple scRNAseq clusters assigned to a hemilineage. For example, hemilineage 0A contains clusters 22, 88 and 112. Of these three, Tj expression is only significant in cluster 88. We generated wild-type MARCM clones of lineage 0A, and one can see that Tj is expressed in a subset of neurons only, presumably cluster 88 (Figure 2F) (37). In contrast, other transcription factors (Fkh, Inv, Mab21a, HLH3b and En) mark all clusters that belong to hemilineage 0A, as revealed by scRNAseq analysis and our immunostaining-based transcription factor expression analysis (Asterisk in Figure 2A; data not shown). In hemilineage 21A, which is composed of only one scRNAseq cluster, Tj marks nearly all cells (Figure 2G). Taken together, these data illustrate how cluster markers identified by scRNAseq data can be used to target individual hemilineages and even distinct subclasses within hemilineages.

Ultimately, we assessed the expression of 23 novel cluster-specific marker genes, all transcription factors, through immunohistochemistry with antibodies against the proteins of interest and/or reporter lines that accurately recapitulate target gene expression (Table 1). This effort allowed us to assign at least one cluster to 15 of the 16 previously unassigned hemilineages in the scRNAseq data (6) (Table 1). This implies that we now have transcription profiles for 33 of the 34 major hemilineages in the VNC, which facilitates the design of lineage-specific split-GAL4 combinations. The only exception is hemilineage 18B, which remains unassigned to any scRNAseq clusters.

Building specific and temporally stable driver lines for hemilineages in the VNC.

To create a split-GAL4 library that uniquely marks essentially all major hemilineages, we generated gene-specific split-GAL4 driver lines by editing the genomic locus of the transcription factors identified above (Figure 3, Figure 3 - figure supplement 1, Key Resources Table, Table 1). To edit the transcription factor locus, we exchanged the intronic cassette of previously engineered MIMIC or CRIMIC lines with a split-GAL4 coding Trojan exon of 13 genes (See Methods). For 11 genes lacking established MIMIC or CRIMIC lines, we used CRISPR/Cas9 mediated gene editing via homology directed repair (HDR) to insert a Trojan exon carrying either DBD or AD split-GAL4 into a coding intron of the target gene and introduced attP sites to facilitate future cassette exchange with any other designer exon via phiC31 mediated cassette exchange (32, 38, 39) (Figure 3 - figure supplement 2). In select cases, we inserted a Trojan exon directly in frame at the 3' end of the gene (Figure 3 - figure supplement 3). In total, we generated 34 split-GAL4 lines for 24 genes, 19 using the MiMIC method and 15 using CRISPR editing (Key Resources Table). The CRISPR approach failed only for *tup* and *E5*.

Comprehensive testing of split-GAL4 combinations to target each hemilineage.

Based on our analysis of scRNAseq data we had clear predictions as to which binary combinations of split-GAL4 lines would label which hemilineages. To test these predictions, we specifically paired these new split-GAL4 lines either with one another, or with previously generated split-GAL4 lines (Table 1) (28, 30, 31). Reconstituted GAL4 was visualized by UAS-myr-GFP or tdTomato and compared to the typical hemilineage morphologies of cell bodies and axonal trajectories to assess whether the split-GAL4 line targeted the predicted lineage. We identified 44 split-GAL4 combinations that target 32 out of 34 hemilineages and summarize the expression pattern of each combination in Table 1. Figure 3 and Figure 3- figure supplement 1 display the larval and adult VNC expression patterns of the driver lines generated for 32 out of 34 hemilineages. Robust expression was also observed in 27 hemilineages in the larva, making these lines suitable for tracking the developmental history of their respective hemilineage during metamorphosis. The expression patterns of the split-GAL4 combinations for the remaining lineages (1B,3B,13A,13B and 24B) start during pupal stages. (1B: *HLH4C*-GAL4^{DBD}, *H15*-GAL4^{AD}; 3B: *H15*-GAL4^{AD}, *ChAT*-GAL4^{DBD}; 13A: *dbx*-GAL4^{DBD}, *dmrt99B*-GAL4^{AD}; 13B: *vg*-GAL4^{DBD}, *d*-GAL4^{AD} or *vg*-GAL4^{DBD}, *tey*-GAL4^{AD}; 24B: *ems*-GAL4^{DBD}, *twit*-GAL4^{AD}, data not shown).

Application of developmentally stable hemilineage specific split-GAL4 lines.

Morphological changes of 4B neurons during development

To show the applicability of our driver lines for developmental studies, we characterized the morphological changes in the neuronal processes during metamorphosis. Neurons of hemilineage 4B are excitatory cholinergic local interneurons (28, 36), and their arborizations are restricted to the ipsilateral leg neuropils and directly synapse with leg motor neurons in addition to many interneurons (1, 17). We have built three different combinations of split-GAL4 lines, each of which specifically targets most, if not all, post-embryonic 4B neurons. Two of these drivers, *ap*-GAL4^{AD} with *fkh*-GAL4^{DBD} and *ap*-GAL4^{AD} with *HLC4C*-GAL4-^{DBD}, drive reporter expression in 4B neurons starting from early larval stages while *ap*-GAL4^{AD} with *HGTX*-GAL4^{DBD} drive robust expression beginning at the white pupal stage (data not shown). Due to its stronger and earlier expression pattern, we used *ap*-GAL4^{AD} with *fkh*-GAL4^{DBD} to mark the morphology of 4B neurons at 0, 3, 12, 24, 48, and 72 hours APF (Figure 4). Like all the other post-embryonic neurons, 4B neurons extend an initial simple neurite bundle after they are born and do not show any further arborization until metamorphosis. As seen in the VNC of a 0-hour APF animal, this initial 4B neurite bundle projects dorsally away from the cell bodies and innervates the leg neuropil diagonally across the dorso-ventral axis (Figure 4A, A'). At 3-hour APF, multiple growth cones that point at different directions are visible on the tip of the 4B bundle (Figure 4B, B'). At 12-hour APF, these growth cones transform into three distinct branches, extending medially, laterally, or dorsally (Figure 4C, C'). At 24-hour APF, finer processes extend from these branches and puncta-like staining are visible, which suggests that synapses are being formed (Figure 4D, D'). At 48-hour APF, the crowded, finer processes are resolved into more refined and discreet processes and the synaptic puncta-like staining becomes more extensive (Figure 4E, E'). At 72-hour APF, the synaptic puncta appear to increase in size and to take a bouton-like shapes, resembling the adult morphology (Figure 4F, F'). In summary, by employing a developmentally stable driver line specific to hemilineage 4B, we documented stepwise morphological changes in the outgrowth of neuronal processes of 4B neurons throughout metamorphosis. These changes occur in distinct phases: initial neurite bundle expansion through new branch additions, followed by the formation and refinement of finer processes and synapses, and concluding with synaptic growth.

Neurotransmitter use

Another use for our library of transcription factor-specific Split-GAL4 lines is to determine which neurotransmitter a specific neuronal population produces. For example, we identified which neurotransmitter Acj6-positive neurons produce. We combined *Acj6*-split-GAL4 with a split-GAL4 line reporting the expression of one of the neurotransmitter marker genes -Gad1, ChAT, or VGlut-

to visualize GABAergic, cholinergic, and glutamatergic Acj6-positive neurons, respectively (Figure 5). Acj6 is known to be expressed in glutamatergic 9B and cholinergic 8B and 23B hemilineages (28). As expected, in each thoracic hemisegment of the VNC, these split-GAL4 combinations marked a single cluster of glutamatergic Acj6-positive neurons corresponding to 9B neurons (arrowheads in Figure 5A), two clusters of cholinergic Acj6-positive neurons corresponding to 8B and 23B neurons (arrowhead and arrows, respectively in Figure 5B), and no GABAergic Acj6-positive neurons (Figure 5C). In each hemibrain, the same split-GAL4 combinations identified one glutamatergic cluster with local projections, several cholinergic clusters with long projections, and two GABAergic clusters with long projections. Additionally, we detected cholinergic Acj6-positive leg and antennal sensory neurons and optic lobe neurons (Figure 5A-C).

Furthermore, one can quickly test if the transcription factor that drives split-GAL4 expression is required for neurotransmitter production. When one inserts Trojan split-GAL4 hemidrivers in the first intron of the transcription factor gene locus, the Hsp70 transcriptional terminator located at the 5' end of the trojan exon prematurely ends the transcript, and the truncated transcription factor oftentimes acts as null mutant. We leverage this to test whether Acj6 has any role in the neurotransmitter identity of these neurons by using *acj6* split lines. We repeated the same experimental procedure in an *acj6* mutant background and found no apparent differences in neurotransmitter expression, concluding that Acj6 is dispensable for neurotransmitter identity (not shown).

In conclusion, we show that one can quickly assay neuronal identity features such as neurotransmitters and their receptors in specific population of neurons in the entire CNS by simply using the split-GAL4 system and intersecting the expression patterns of a lineage specific gene with the expression of another gene coding for neuronal identity. However, care should be taken interpreting these results, as the presence of the Hsp70 transcriptional terminator at the 5' end of the Trojan exon may also affect the host gene's 3' UTR regulation, such that these drivers do not always faithfully recapitulate expression of genes subject to post-transcriptional regulation as was observed for ChAT (28, 40).

Behavioral analysis with targeted lineage manipulation

Understanding the functional roles of specific hemilineages in the VNC is crucial for unraveling the neural circuits that govern behavior, yet the tools to study these lineages in detail have been limited. Harris *et al*.(19) developed genetic tools to mark and track a small subset of VNC

hemilineages through metamorphosis into the adult. This work used thermogenetic methods to stimulate neuronal activity of specific hemilineages to assess their function. This was done with decapitated flies to remove the effect of driver line expression in the brain. However, for many hemilineages, either no driver line existed or only a small portion of a hemilineage was targeted. To overcome these issues, we use our new split-GAL4 combinations to manipulate eight hemilineages for which no drivers previously existed (0A, 1B, 4B,8B, 9B, 14A, 16B, 17A) and to target 16 lineages studied by Harris *et al*., (19) with better coverage (Table 2). We evaluate lineage-coupled behavior with optogenetic activation, a method that is more robust and has a better time resolution compared to thermogenetic activation (41). We show below how this approach is compatible with genetic methods to remove unwanted GAL4-mediated gene expression in the brain by applying a teashirt/FLP based genetic intersection with the LexA/LexAop system to restrict GAL4 expression to the VNC (42). A major advantage of such layered genetic set-up is that behavior can be evaluated in intact flies without the need for decapitation. The lineage-behavior analysis of the 26 hemilineages are summarized in Table 2. Recordings of intact and decapitated are available as Supplemental Videos and the video number corresponds to the hemilineage name. In the sections below we summarize four examples.

<u>Hemilineage 8B</u>

Hemilineage 8B neurons, which are cholinergic and excitatory, show complex segment-specific intersegmental projections that innervate the tectulum and leg neuropil (36). To target 8B neurons, we used *lim3*-GAL4^{DBD} and *c15*-GAL4^{AD}, which target most of the 8B neurons as well as numerous neuronal clusters in the brain (Figure 6A). We activated only 8B neurons through exclusion of brain neurons by layering *lim3*-GAL4^{DBD}, *c15*-GAL4^{AD} with a *teashirt (tsh)* driver that restricts expression of the optogenetic construct CsChrimson-mVenus to only VNC neurons (42) (Figure 6B). We observed that optogenetic stimulation of 8B neurons triggered jump behavior in intact and decapitated animals (Figure 6C, D, Video-8A-1;Video-8A-2). Unlike 7B neuronal activation, which makes flies raise their wings before jumping (Video-7B-1;Video-7B-2;Video-7B-3) (20), 8B activation resulted in jumping without a wing raise, which is reminiscent of the Giant Fiber (GF) induced escape movement sequence (43-47).Therefore, our results suggest that 8B neurons participate in the GF-driven take-off circuit.

To investigate the relationship between 8B and the GF neurons, we analyzed the synaptic connections of the GF (DPN01) using MANC2.1 in neuPrint (1, 48, 49), and focused on neurons with at least five synapses, for one half of the bilateral symmetric circuit. We found that hemilineage 8B neurons are upstream synaptic partners of the GF, with 12 8B neurons

accounting for 12.5% of the GF synaptic inputs (Figure 6- figure supplement 1, Figure 6- figure supplement Table 1). Surprisingly, 8B neurons were also downstream synaptic partners of the GF, with 13 neurons accounting for 12.5% of the GF's synaptic outputs (Figure 6- figure supplement 2, Figure 6- figure supplement Table 2). This contribution is significant, as it is even higher than the 8.7% of synaptic output connections that a GF dedicates to innervating the tergotrochanter motor neuron (TTMn), which innervates the jump muscle. We next compared if those 8B neurons that are downstream partners of the GF also provide input to the GF. Surprisingly, the majority of 8B neurons that connect to the GF are both downstream and upstream synaptic partners. These 9 neurons make up 21.5%. and 9.1% of total GF synaptic inputs and outputs, respectively. Taken together our behavioral data and the connectome analysis suggest that a subset of 8B neurons function in the GF circuit and elicit take-off behavior.

Hemilineage 9A

Hemilineage 9A is composed of inhibitory GABAergic neurons, which integrate sensory input from leg proprioceptive neurons (18, 28). To activate 9A neurons, we drove CsChrimson expression with *Dr*-GAL4^{AD} and *gad1*-GAL4^{DBD}. Decapitated animals exhibited erratic walking behavior with their legs extended when the stimulus lasted over three seconds, and this erratic walking immediately stopped when the stimulus ended (Figure 6E, Video-9A-1; Video-9A-2; Video-9A-3). In agreement with previous reports (18, 19), we observed that both decapitated and intact animals extended their legs in response to activation.

Hemilineage 12A

Hemilineage 12A neurons are cholinergic and excitatory, and display segment-specific and complex intersegmental projections to wing and leg nerve bundles (1, 17). We used the *unc-4*-GAL4^{DBD} and *TfAP2*-GAL4^{AD} driver line to express CsChrimson in 12B neurons. None of these animals, however, survived to adulthood, not even in the absence of retinal, the cofactor required for CsChrimson activity. To overcome this issue, we generated stochastic FLP-based lineage clones that expressed CsChrimson in 12A neurons in one or a few hemisegment(s). We then optogenetically activated decapitated flies and recorded their behavior (Video-12A-1; Video-12A-2), followed by dissection and immunostaining to visualize which lineage clones were responsible for the observed phenotype. We found two cases where optogenetic activation resulted in bilateral wing opening and a leg swing. The segment and side of the 12A lineage clone corresponded to the side of the leg that moved (Figure 6F, G). We also observed the following behavioral phenotypes in response to optogenetic activation, but we did not dissect the animals to further

identify the lineage clone: high frequency wing beating, backward walking immediately after the stimulus termination, and abdominal extension and bending. These results indicate that 12A neurons, as expected from their complex projections, control a magnitude of behaviors.

Hemilineage 21A

Hemilineage 21A neurons are glutamatergic, likely inhibitory interneurons, and innervate the leg neuropil in all thoracic segments. To assess the behaviors executed by 21A neurons, we used two different driver lines: *Dr*-GAL4^{AD} and *ey*-GAL4^{DBD} or *Dr*-GAL4^{AD} and *tj*-GAL4^{DBD}. Both combinations target most of the 21A neurons, the latter with higher specificity, yet both lines showed consistent results upon optogenetic activation. Stimulation of either intact or decapitated animals forced the leg segments in a specific geometry (Video-21A-1; Video-21A-2). In tethered intact animals, whose legs are freely moving in the air, we observed a clear flexion in the femur-tibia joint (Figure 6H-J). To test whether 21A neurons are necessary for the relative femur-tibia positioning, we eliminated 21A neurons by expressing UAS-*hid* with *Dr*-GAL4^{AD}, *ey*-GAL4^{DBD}. Flies lacking 21A neurons showed aberrant walking patterns. We observed that femur-tibia joints of the hind legs protruded laterally compared to the control sibling flies (Figure 6, K, L). Our results showed that 21A neurons control the relative positioning of the leg segments, especially the femur and tibia.

Other anatomical region of interest

While characterizing the expression pattern of the gene-specific split-Gal4 library, we noted that applicability of these tools extends beyond the VNC. A total of 24 driver lines targeted clusters of neurons in the suboesophageal zone (SEZ) (Table 1). The SEZ processes mechanosensory and gustatory sensory input and controls motor output related to feeding behavior. It is anatomically part of the VNC and comprises the first three segments of the VNC, which are populated by NBs that are the segmental homologs of NBs found in the thoracic and abdominal segments of the VNC (50-52). A key difference is that only a small number of NBs pairs survive in the SEZ (35). The SEZ NBs are expected to express a similar set of transcription factors as their thoracic counterparts. Therefore, these transcription factors and their corresponding split-GAL4 driver lines are excellent tools to target and manipulate homologous lineages in the SEZ.

Discussion

The ability to trace neuronal lineages across their developmental journey and to manipulate their function is essential to investigate how neurons interconnect to form neuronal circuits and regulate specific behaviors. To address these questions, most studies have focused on a few specific regions of the CNS, e.g., the mushroom body in flies, for which specific genetic tools exist to target defined neuronal populations during developmental and adult life. In this study, we utilized scRNAseq data from the VNC (6) completed its annotation for all but one hemilineage, and analyzed the transcriptome of individual hemilineages. Through this effort, we identified new marker genes for hemilineages, verified their expression patterns in the VNC, and created split-GAL4 driver lines for 24 lineage-specific marker genes lines by editing their genomic loci. By employing binary combinations of these new lines amongst each other or with driver lines established previously, we constructed a comprehensive split-GAL4 library that targets 32 out of 34 hemilineages during development and adult life (Table 1), enabling the genetic dissection of how each hemilineage contributes to circuit development (28, 30 2020 #25, 31, 53, 54).

Mapping and manipulating morphological outgrowth patterns of hemilineages during development

The driver line combinations presented here are developmentally stable and most combinations label both embryonic and post-embryonic neurons of the target hemilineage. This makes them a valuable resource for lineage-based dissection of larval nervous system development and function. Furthermore, they target individual hemilineages throughout metamorphosis and adult life. This is critical as the formation and maturation of adult neuronal circuits takes place during metamorphosis and last several days. This time window is greatly prolonged compared to the rapid development of larval circuits that occurs within a few hours during embryogenesis and offers greater opportunities for experimental manipulation. By layering temperature or light controlled genetic effectors, like shibere^{TS}, channelrhodopsins or LACE-Cas9 (55, 56) with our toolkit, researchers can manipulate neuronal and gene activity with high temporal resolution. This makes it possible to investigate dynamic processes such as synapse formation, circuit assembly, and functional maturation. For example, recent studies demonstrated that developing neuronal circuits exhibit patterned calcium activities during metamorphosis and these activities likely regulate the synaptic connectivity among neurons (57, 58). Shibere^{TS} expression driven by our driver lines can inhibit the developmentally observed neuronal activity in a specific hemilineage

during a specific time window to test whether this manipulation alters the synaptic connectivity of the hemilineage.

8B neurons likely function in the giant-fiber escape circuit

Our work here demonstrated that the activation of 8B neurons elicits robust take-off behavior that closely resembles the GF induced take-off response (46). This observation raises an intriguing question: do 8B neurons function in the GF escape circuit? Interestingly, although 8B neurons do not appear to connect directly to TTMns, the primary output neurons of the escape circuit (1), we report that they do form a complex synaptic relationship with the GF. Specifically, a subset of 8B neurons is both upstream and downstream synaptic partners of the GF, accounting for 25% of GF's synaptic input and 12.5% of GF's output. This synaptic loop centered around the GF neurons suggests a recurrent feedback mechanism within the GF circuit. Given that hemilineage 8B neurons exhibit interconnectivity with each other and receive leg proprioceptive input (1), we speculate that lineage 8B may function as an integrator in and amplifier of the GF circuit. This example underscores that our split-GAL4 library provides an excellent resource for further exploration of lineage-coupled behavior.

Addressing lineage differentiation by studying cell heterogeneity within hemilineages

Our lineage annotation of the VNC transcriptome revealed that most hemilineages are represented by more than one RNAseq cluster, which reflects heterogeneity within a hemilineage and indicates that hemilineages can be further subdivided into subclasses of neurons. Indeed, we found that such subclasses express specific transcription factors, which can be considered subclass-defining factors, for example Tj in hemilineage 0A (Figure 2F). The tools we present here form a starting point to visualize or manipulate neuronal subclasses within a hemilineage. For example, one can use the split-GAL4 driver line combinations to express an UAS transgene preceded by an FRT-flanked stop codon in a specific lineage. Flippase expression can be easily restricted to a subclass of neurons in a hemilineage with the LexA/LexAop system under control of the subclass-defining transcription factor. As a result, the transgene will only be expressed in a subclass of neurons in a hemilineage. Instead of working with subclass-defining transcription factors, one can also use birth-order marking temporal genes such as *chinmo*, *mamo*, or *broad-c* (59-62) to restrict driver activity to a group of neurons born in a specific temporal window within a hemilineage. Thus, with a strategic combination of orthogonal gene specific driver system (e.g.,

split-GAL4, LexA, and QF), one can now dissect the neuronal circuit formation with unprecedented precision.

In conclusion, our study underscores the potential of temporally stable driver lines to target hemilineages in the VNC during development and adult life. This approach enables future studies investigating how neurons acquire their specific fates and integrate into the broader networks of neural networks that control intricate animal behaviors.

Materials and Methods

scRNA-seq data analysis

Candidate genes to convert into split-GAL4 driver lines were identified using the scRNA-seq data generated by Allen *et al.*, 2015. No modifications were made to the preprocessing pipeline, and we used the cluster markers defined by Allen *et al*, (6) and investigated the combinatorial expression patterns of the highest expressed cluster markers in binary combinations using the code shared on GitHub using Seurat v5. Candidate genes to make split-GAL4 drivers from were chosen based on their ability to selectively mark the scRNAseq cluster(s) covering a hemilineage, and selected markers that were expressed by near all cells of the hemilineage for the downstream experimental validation steps. We then prioritized testing these combinations based on the availability of antibodies, BAC lines and CRiMIC/MiMIC constructs to validate their expression pattern prior to creating split-GAL4 lines for these candidates.

Fly stocks and behavioral experiments

Fly stocks were reared on the standard cornmeal fly food at 25°C unless indicated otherwise. Fly lines used in this study are listed in the Key Resources Table. A current inventory of gene-specific split-GAL-4 lines is maintained by Yu-Chieh David Chen and Yen-Chung Chen from Claude Desplan's lab (https://www.splitgal4.org). Lines were contributed by the labs of Claude Desplan, Liqun Lue, Benjamin White, Norbert Perrimon and Haluk Lacin's laboratories. Behavior was tested at room temperature (22–25°C) 2–10 days post-eclosion.

Clonal Analysis

Wild type MARCM analysis was performed as described before (37). Animals were heat-shocked within 24 hours after egg hatching (27). Multi-Color FLP-Out NB3-5 (lineage 9) clones were generated with 49C03-GAL4 crossed to hsFlp2::PEST;; HA_V5_FLAG as described before (29, 63). 20X-UAS>dsFRT> CsChrimson mVenus_attp18, hs-Flp2PESt_attp3 X Tf-AP2-GAL4: lineage clones were generated via heat-shock within 24 hours window after egg hatching.

Gene editing

Introduction of Trojan split-GAL4 by Recombinase Mediated Cassette Exchange.

Gene-specific split-GAL4^{AD} and split-GAL4^{DBD} lines were made from MiMIC or CRIMIC lines via Trojan exon insertion as described before (28, 31, 32, 38). Briefly, pBS-KS-attB2-SA(0,1, or 2)-T2A-Gal4DBD-Hsp70 or pBS-KS-attB2-SA(0,1, or 2)-T2A-p65AD-Hsp70 were co-injected with

phiC31 integrase into the respective MiMIC/CRIMIC parent stock (Key Resources Table). Transformants were identified via the absence of y+ or 3xP3-GFP markers. The correct orientation of the construct was validated by GFP signal upon crossing the putative hemidriver to a line carrying the counter hemidriver under control of the tubulin promoter and an UAS-GFP transgene (Key Resources Table).

Insertion of gene-specific Trojan split-GAL4 construct with CRISPR

Guide RNAs (gRNA) were selected to target all expressed isoforms in an amendable intronic region or to the 3' end of the gene if no suitable intron was present (e.g., *fer3 and ems*) (Key resources Table, Supplemental Methods Table 1). gRNAs were identified with CRISPR target Finder for vas-Cas9 flies, BDSC#51324 with maximum stringency and minimal off-target effects (Supplemental Methods Table 1) (64). gRNA targeting *hb9, vg,* and *H15* were cloned into pCFD4 together with a guide RNA to linearize the donor vector (65, 66). The remainder of the guides were synthesized into pUC57_GW_OK2 (Genewiz/Azenta (Burlington, MA)).

CRISPR donors were generated using a modified version of the strategy developed by Kanca *et al.* (67). We used the Genewiz company to synthesize a DNA fragment into the EcoRV site of the pUC57-GW- OK2 vector. This fragment is made of the left and right homology arms (HA) which are immediately adjacent to the gRNA cut site and restriction enzyme sites (SacI-KpnI) between these arms (Supplemental Methods Figure 1A). We then directionally cloned the Sac1-attP-FRT-splitGAL4-FRT-attP-KpnI fragment (Supplemental Methods Figure 1B) in between the left and right HAs using the SacI and KpnI sites. Note that SacI and Kpn should only be chosen when the homology arms do not have these cut sites. To facilitate this last step, we generated universal plasmids in each reading frame for each hemi driver, DBD and p65.AD in the original Trojan vector backbones, referred to as pBS-KS-attP2FRT2-SA-T2AGAL4[AD or DBD (0,1,2)]-Hsp70 with Gibson assembly, combining the following fragments:

(i) pBS-KS backbone from the original Trojan vector (digested with SacI and KpnI).
(ii) the exon (consisting of splice acceptor, GAL4-DBD or p65.AD, and Hsp70 Poly A signal) was PCR-amplified from the original Trojan vectors (e.g., pBS-KS-attB2-SA(0)-T2A-p65AD-Hsp70) with the following primers:

F: 5' *ctagaaagtataggaacttc*GAATTC**agtcgatccaacatggcgacttg** 3'

R:5' *ctttctagagaataggaacttc*GATATC**aaacgagtttttaagcaaactcactcc** 3

Note EcoRI and EcoRV (capitalized) sites were included as a back-up strategy for replacing the Trojan exon between attP FRT if needed.
(iii) 5' SacI-attP-FRT sequence was PCR amplified from pM14 (67) with primers:

F: 5' <u>actcactatagggcgaattgGAGCTC</u>*acggacacaccgaag* 3'

R: 5' *caagtcgccatgttggatcgac 3'*

(iv) 3' FRT- attP-KpnI sequence PCR amplified from pM14 (67) with primers:

F: 5' **ggagtgagtttgcttaaaaactcgtt**tGATATC*gaagttcctattctctagaaag* 3'

R: 5' <u>cactaaagggaacaaaagctgggtacc</u>*gtactgacggacacaccgaag 3'*

Corresponding sequences from pBS-KS are underlined, pM14 are in italics, and Trojan AD/DBD are in bold; restriction enzyme sites are in all caps. All plasmids were validated by Sanger sequencing (Genewiz/Azenta (Burlington, MA).
Note that for *hb9, vg, sens-2, H15, scro, Ets21C* and *eve* we inserted the T2A- split-GAL4^{DBD} and/or T2A-split-GAL4$^{p65\text{-}AD}$ into the host gene intron as a Trojan exon with flanking FRT sites in a similar manner to CRIMIC lines generated by the Bellen Lab (detailed below). However, since this is problematic for FLP-dependent mosaic experiments we generated additional lines for *hb9, sens2, Ets21C eve* and *vg* lacking FRT sites by replacing the FRT flanked cassettes with the original White lab Trojan AD/DBD exons via attP-phiC31 mediated recombination as described above.

Split-GAL4 drivers for and D were made by the Erclick laboratory. CRISPR-mediated gene-editing was performed by WellGenetics Inc. using modified methods of Kondo and Ueda (68). For *fkh*, the gRNA sequence GTGACATCACCAATACCCGC[TGG] was cloned into a U6 promoter plasmid. Cassette T2A-Gal4DBD-RFP, which contains T2A, Gal4DBD, a floxed 3xP3-RFP, a Hsp70Ba 3'UTR, and two homology arms were cloned into pUC57-Kan as donor template for repair. *fkh/CG10002*-targeting gRNAs and hs-Cas9 were supplied in DNA plasmids, together with donor plasmid for microinjection into embryos of control strain w[1118]. F1 flies carrying selection

marker of 3xP3-RFP were further validated by genomic PCR and sequencing. CRISPR generates a break in fkh/CG10002 and is replaced by cassette T2A-Gal4DBD-RFP.

Similarly, for *D*, the gRNA sequences ACTCGACTCTAATAGAGCAC[CGG] /GCACCGGAACCGGTCGCCTC[AGG] were cloned into U6 promoter plasmid(s). Cassette T2A-VP16AD-3XP3-RFP, which contains T2A, VP16AD, and a floxed 3xP3-RFP, and two homology arms were cloned into pUC57-Kan as donor template for repair. *D/CG5893*-targeting gRNAs and hs-Cas9 were supplied in DNA plasmids, together with donor plasmid for microinjection into embryos of control strain w[1118]. F1 flies carrying selection marker of 3xP3-RFP were further validated by genomic PCR and sequencing. CRISPR generates a break in *D/CG5893* and is replaced by cassette T2A-VP16AD-3XP3-RFP.

Direct split-GAL4 insertion with CRISPR

For *fer3, ems* and *HLH4C,* we inserted T2A-GAL4^{DBD} directly in frame with the last coding exon instead of inserting it into an intron as a Trojan exon flanked by attP and FRT sites. The gRNA and entire donor region (a LHA-GAL4-DBD-RHA fragment, without attP and FRT sequences) were synthesized in pUC57_gw_OK2, and injected into vas-Cas9 flies (w[1118]; PBac(y[+mDint2]=vas-Cas9)VK00027) by Rainbow transgenics (Camarillo, CA). Transformed animals were crossed to flies carrying Tubulin-GAL4^{AD}, UAS-TdTomato and offspring was scored for TdTomato expression to identify positive lines. The expression pattern of the reporter served as a verification for correct editing events; no further verification was performed.

Immunochemistry and Data Acquisition

Samples were dissected in phosphate buffered saline (PBS) and fixed with 2% paraformaldehyde in PBS for an hour at room temperature and then washed several times in PBS-TX (PBS with 1% Triton-X100) for a total 20 min. Tissues were incubated with primary antibodies (Key Resources Table) for two to four hours at room temperature or overnight 4°C. After three to four rinses with PBS-TX to remove the primary antisera, tissues were washed with PBS-TX for an hour. After wash, tissues secondary antibodies were applied for two hours at room temperature or overnight at 4°C. Tissues were washed again with PBS-TX for an hour and mounted in Vectashield or in DPX after dehydration through an ethanol series and clearing in xylene (69). Images were collected with 20X or 40X objectives using confocal microscopy. Images were processed with Image J/FIJI.

Behavioral Analysis

For optogenetic stimulation, we used standard food containing 0.2 mM all-trans retinal. As a light source for optogenetic activation, we used either white light coming from the gooseneck guide attached to the halogen light box or red light (Amazon-Chanzon, 50W, Led chip,620nm - 625nm / 3500 - 4000LM). Animal behaviors were recorded via a USB based Basler Camera (acA640-750um) under continuous infrared light source (Amazon-DI20 IR Illuminator).

Acknowledgements

We thank the Lacin laboratory members for critical reading of the manuscript, discussion and suggestions. We thank Aaron Allen and Stephen Goodwin for sharing their code for scRNAseq data analysis and sharing their fly lines prior to publication and Dorothea Godt, Angelike Stathopoulos and Gerald Campbell for gifting antibodies. We also thank Hugo Bellen and Oguz Kanca for sharing their reagents. Many stocks obtained from the Bloomington Drosophila Stock Center (NIH P40OD018537) were used in this study as well as antibodies from the Developmental Studies Hybridoma Bank, created by the NICHD of the NIH and maintained at the University of Iowa, Department of Biology, Iowa City, IA 52242.

Funding:

This work was supported by grants from the National Institutes of Health to Y.C.D.C (F32EY032750 and K99EY035757), J.B.S. (R01NS036570), and to H.L. (R01NS122903), and by funding from HHMI to J.W.T.

Figure Legends

Figure 1: Intersecting the expression of *acj6* and *unc-4* genes with the split-GAL4 method faithfully marks hemilineage 23B.

(A-C) Projections of confocal stacks of the adult VNC. Blue: CadN; **(A)** *acj6*-GAL4 driven nls-tdTomato expression (displayed in green) marks Acj6 expressing neurons**. (B)** *unc-4*-GAL4 driven nls-tdTomato expression (displayed in green) marks Unc-4 expressing neurons. **(C)** The intersection of acj6 and unc-4 expression (displayed in green) (*acj6*-GAL4^{AD}, *unc-4*-GAL4^{DBD}> UAS-nls-tdTomato) marks lineage 23B neurons in the SEZ and VNC**. (D)** A partial confocal projection showing the complete overlap between membranous GFP (green) and Acj6 (magenta) immunostainings in *acj6*-GAL4^{AD}, *unc-4*-GAL4^{DBD}-marked 23B neurons in the adult VNC (T1 and T2 segments shown). **(E)** scRNAseq t-SNE plot shows Acj6 (Purple) and Unc-4 (Dark Blue) co-expression in a group of cell clusters.

Figure 1 - figure supplement 1: *acj6*-GAL4^{AD}, *unc-4*-GAL4^{DBD}-driven myr-GFP marks 23B neurons throughout development.

(A, B) Acj6 (blue) and Unc-4 (magenta) co-expression shows robust overlap in GFP-marked embryonic progeny of NB7-4, 23B neurons, in a late-stage embryo. **(C-D)** Acj6 (blue) expression marks 23B neurons in an early stage larval VNC **(C)** and an early stage pupal VNC **(D).** The only lineages that express Acj6 are 23B, 8B and 9B, and of these only the posterior-dorsal cells, corresponding to hemilineage 23B, co-stained for GFP and Acj6 in the larval and pupal VNC**. (E)** This driver combination marks a cluster of SEZ neurons (arrowhead) in the adult brain, presumably SEZ 23B neurons in addition to sensory neuron afferents (arrows). **(F)** Close up of SEZ to highlight the corresponding cell bodies (arrowhead).

Figure 2: Matching the scRNAseq clusters to hemilineages.

(A-C) Confocal stack of larval VNC displaying the overlapping expressions between transcription factors identified from scRNAsec data (Fkh, Kn, and Sp1; green in **A**, **B**, and **C**, respectively) and Hb9 (magenta) in three lineages: 4B, 10B, and 16B (dashed lines). Asterisk in A indicates the Fkh^{+}Hb9^{-} 0A lineage neurons. **(D)** Sox21a-GAL4 driven UAS-GFP (green) marks lineage 2A neurons **(E)** Hmx^{GFSTF} reporter (green) marks lineage 17A neurons. **(F, G)** Wild-type MARCM clones (green) immunostained for Tj (magenta). The insets show the clone location in the VNC counterstained with CadN (blue) **(F)** Tj marks subpopulations of neurons in lineage 0A in the T2 segment. These neurons likely belong to cluster 88, the only Tj^{+} 0A cluster in scRNAsec data. **(G)**

Tj marks nearly all neurons of lineage 21A in the T1 segment. Lineage identification of MARCM clones were performed based on neuronal projections detailed in Truman *et al.,* 2004 (66). scRNAseq clusters with the corresponding lineages shown under each panel. Only one thoracic segment shown. Neuroglian specific antibody BP104 labels axon bundles of all lineages (magenta in D-E).

Figure 3: The VNC expression of select driver lines from the split-GAL4 library targeting individual hemilineages.

Projections of confocal stacks showing the expression pattern of split-GAL4 driven membranous GFP (green) in the larval (**A-O)** and adult VNC **(A'-O')**. Only thoracic segments are shown in the larval images **(A, A')** Hemilineage 0A, marked by *inv*-GAL4-DBD, *tj*-VP16.AD. **(B, B')** Hemilineage 1A marked by *ets21c*-GAL4-DBD, *Dr*-p65.AD. **(C, C')** Hemilineage 2A marked by sox21a GAL4-DBD, *VGlut*-p65.AD. **(D, D')** Hemilineage 4B marked by *ap*-p65.AD, *fkh*-GAL4-DBD. **(E, E')** Hemilineage 5B marked by *vg*-p65.AD, *toy*-GAL4-DBD. **(F, F')** Hemilineage 6B marked by *sens2*-p65.AD, *vg*-GAL4-DBD. **(G, G')** Hemilineage 7B marked by *mab21*-GAL4-DBD, *unc-4*-p65.AD. **(H)** Hemilineage 8A marked by *ems*-GAL4-DBD, *ey*-p65.AD**. (I, I')** Hemilineage 8B marked by *lim3*-GAL4-DBD, *C15*-p65.AD**. (J, J')** Hemilineage 9A marked by *Dr*-p65.AD, *gad1*-GAL4-DBD. **(K, K')** Hemilineage 9B marked by *acj6*-p65.AD, *VGlut*-GAL4-DBD. **(L, L')** Hemilineage 10B marked by *knot*-p65.AD, *hb9*-GAL4-DBD. **(M, M')** Hemilineage 12A marked by *TfAP-2*-GAL4-DBD, *unc-4*-p65.AD. **(N, N')** Hemilineage 14A marked by *Dr*-p65.AD, *toy*-GAL4-DBD. **(O, O')** Hemilineage 17A marked by *unc-4*-p.65AD, *hmx*-GAL4-DBD.

The VNC was counterstained with CadN (magenta). The target lineage is indicated on the left bottom corner of each panel. Z-projections were made of selected regions of the VNC to highlight the cell-body clustering and axonal budling.

Figure 3 - figure supplement 1: The rest of the driver lines from the Split-GAL4 library targeting individual hemilineages.

Projections of confocal stacks showing the expression pattern of Split-GAL4-driven membranous GFP (green) in the larval (**A-O)** and adult VNC **(A'-O')**. Only thoracic segments shown in the larval images. **(A)** Hemilineage 1B marked by *HLH4c*-GAL4-DBD, *H15*-p65.AD. **(B)** Hemilineages 3A, 7B, and 12A are marked by *H15*-p65.AD, *ChAT*-GAL4-DBD. **(C)** Hemilineages 3B and 12B marked by *fer3*-GAL4-DBD, *cg4328*-AD**. (D)** Hemilineage 6A marked by *mab21*-p65.AD, *toy*-GAL4-DBD. **(E)** Hemilineage 11A marked by *unc-4*-GAL4-DBD, *tey* VP16.AD. **(F)** Hemilineage 11B marked by *eve*-p65.AD, *gad1*-GAL4-DBD. **(G)** Hemilineage 12B marked by *HGTX*-GAL4-

DBD, *gad1*-p65.AD. **(H)** Hemilineage 13A marked by *dbx*-GAL4-DBD, *dmrt*-p65.AD. **(I)** Hemilineage 13B marked by *vg*-GAL4-DBD, *D*-vp16.AD. **(J)** Hemilineage 15B marked by *HGTX*-GAL4-DBD, *VGlut*-p65.AD. **(K)** Hemilineage 16B marked by *hb9*-p.65AD, *VGlut*-GAL4-DBD. **(L)** Hemilineage 19A marked by *dbx*-GAL4-DBD, *scro*-p65.AD. **(M)** Hemilineage 20/22A marked by *bi*-GAL4-DBD, *shaven*-p65.AD. **(N)** Hemilineage 23B marked by *unc-4*-p65.AD, *acj6*-GAL4-DBD. **(O)** Hemilineage 24B marked by *twit*-p65.AD, *ems*-GAL4-DBD.

Figure 3 - figure supplement 2. CRISPR mediated insertion of Trojan Exons.

(A) Construction of CRISPR donor plasmids. For each gene of interest (GOI) a fragment is synthesized into EcoRV restriction site of pU57_gw_OK2 as described before (64). Briefly, this fragment contains a small sequence of the tRNA spacer, the gRNA against the gene of interest (GOI) (turquoise) and the Left HA and Right HA (turquoise) separated by a spacer containing *SacI* and *KpnI* restriction sites (black). A hemidriver cassette (gray, also see B) flanked by *SacI* and *KpnI* restriction sites is directionally cloned in between the HAs**. (B)** Six plasmids containing hemidriver cassettes (gray box) flanked by *SacI* and *KpnI* were made in the pBS-KS plasmid backbone. Each plasmid contains either a split-GAL4-DBD or p65.AD in phase 0, 1 and 2. Each hemidriver furthermore contains a 5'attP and FRT sequences, followed by a linker, splice acceptor (SA) and T2A proteolytic cleavage site. The linker length varies to keep the hemidriver in phase with the preceding exon (linker length: 24 nucleotides phase 0, 41 nucleotides phase 1 or 40 nucleotides phase2). A hsp70 termination sequence is introduced at the 3'end of the hemidriver followed by a splice donor (SD), FRT, and attP sequence. Note that the DBD cassettes do not contain a splice donor to keep them consistent with previously published split-GAL4 Trojan exon donors (28). **(C)** The HAs promote HDR and the entire hemidriver cassette is inserted at the site of the CRISPR/CAS9 cut, targeted by recognition sequence the gRNA-GOI. The attP sites allow for future cassette exchange with RMCE and genetic crosses.

Figure 3 - figure supplement 3. Direct tagging with CRISPR.

Schematic representation of the direct tagging method that establishes split-GAL4^{DBD} lines without any cloning.

The gRNA against the gene of interest (GOI) cuts in the direct vicinity of the stop codon (+/- 20 nt). The left HA 3' end reaches up to, but does not include the stop codon, and the right HA 5' end starts at the first nucleotide of the 3' UTR. This ensures that the T2A-DBD fragment will be inserted at the 3' end of the gene and is translated in frame with the GOI. **(A)** Construction of the CRISPR donor for direct tagging. A fragment that contains a small portion of the tRNA spacer, the gRNA-

GOI, and the LHA, T2A-DBD and RHA sequence is directly synthesized into the EcoRV site of pU57_gw_OK2. **(B)** Upon embryo injection, expression of gRNA1 linearizes the donor constructs and the LHA-T2A-DBD-RHA fragment is used for CRISPR/Cas9 guided HDR. As a result, the T2A-DBD is inserted in frame at the 3' end of the gene, and endogenous 3' UTR posttranslational regulation mechanisms remain intact.

Figure 4: Neurons of hemilineage 4B show profound morphological changes during development.

Projection of confocal stacks showing the morphology of 4B neurons (green) marked with the *ap*-GAL4^{AD} and *fkh*-GAL4^{DBD} driver combination across different developmental time points during metamorphosis: 0, 3, 12, 24 and 48 hours after puparium formation (APF). The VNC is counterstained with CadN (magenta). Cell bodies of 4B neurons in the T3 region are marked with asterisks. **(A-F)** Complete projections in T2-T3 segments. Anterior (A) up; posterior (P) down. **(A'-F')** Transverse views of the entire T3 segments across the dorso-ventral (D-V) axis; Dorsal is up**.** Arrowheads in B' mark growth cones. Arrowheads in C' mark three new branches towards the medial (m), lateral (l) and dorsal (d) part of the leg neuropil.

Figure 5: Acj6-positive neurons in the VNC are glutamatergic or cholinergic.

(A-C) Split-GAL4 line reporting Acj6 expression intersected with a cognate split-GAL4 line reporting the expression of Gad1, ChAT or VGlut to visualize GABAergic, cholinergic, and glutamatergic populations of Acj6-positive neurons, respectively. The VNC is counterstained with CadN (magenta). **(A)** Split-GAL4 combination *acj6*-GAL4^{AD}, *gad1*-GAL4^{DBD}>UAS-GFP driven UAS-GFP shows that the optic lobes contain cholinergic Acj6-positive neurons in addition to a few clusters of neurons with prominent long projections. In the VNC, two cholinergic clusters per hemisegment corresponding to 8B (arrowheads) and 23B (arrows) hemilineages are labeled in addition to some sensory neurons (asterisks). **(B)** Split-GAL4 combination *acj6*-GAL4^{AD}, *VGlut*-GAL4^{DBD}> UAS-GFP marks a single glutamatergic lineage in the dorsal part of the brain and one 9A glutamatergic cluster in the VNC. **(C)** Split-GAL4 combination *acj6*-GAL4^{AD}, *gad1*-GAL4^{DBD}>UAS-GFP marks two GABAergic lineages in the brain and nothing in the VNC.

Figure 6: Behavioral analysis with targeted lineage manipulation.

(A-D) Optogenetic activation of hemilineage 8A in the VNC triggers jump behavior. *lim3*-GAL4^{DBD}; *c15*-GAL4^{AD} driven CsChrimson::mVenus (green) targets 8B neurons in the VNC but also shows an unwanted broad brain expression **(A),** which can be suppressed via an additional layer of

intersection using teashirt (tsh)-lexA driven FLP strategy **(B)**. **(C, D)** Overlay of video frames to capture the jump sequence induced by optogenetic activation of lineage 8B in the VNC. Intact flies **(C)** and decapitated flies **(D)** jump without raising their wings upon optogenetic activation, but decapitated flies were slower to initiate the jump. **(E)** Optogenetic activation of hemilineage 9A induces forward walking in decapitated flies. **(F, G)** Clonal stimulation of hemilineage 12A in the VNC in decapitated flies induces bilateral wing opening and single-step behavior. **(F)** Confocal stack displaying the lineage 12A clone that extends from T2 into T1 and T3. **(G)** Overlay of movie frames. The fly folds both wings outward and swings its right front leg forward upon optogenetic activation. **(H, L)** Optogenetic activation of hemilineage 21A in the VNC on a tethered, intact fly triggers flexion of the tibia-femur joint. **(H)** Without stimulus, all the legs move erratically in response to being tethered. **(I)** Upon optogenetic activation, all legs are pulled toward the body, the tibia-femur joints are flexed, and animals stay in this position until the end of stimulus. **(J)** Overlay of the movie shown in panel H and I, zoomed in on the left T1 leg. Note how the leg is pulled towards the body upon activation (520 msec) compared to its more lateral position without activation (315 msec). **(K, L)** Elimination of 21A neurons makes hind leg femur-tibia joints protrude laterally **(L)** compared to control animals **(K).** For all overlays of movies, green display frames without optogenetic activation, magenta with optogenetic activation.

Figure 6 - figure supplement 1: Giant Fiber (GF) Connectome.

Synaptic connectivity of the GF neuron extracted from the data generated by Marin et al., (1). **(A-C)** Analysis of GF input connections. **(D-F)** Analysis of GF output connections. **(A)** Count of neurons per hemilineage that form synapses with GF dendrites. A total of ten hemilineages form synapses with GF dendrites. Five neurons originate from hemilineage 8B, six from hemilineage 7B, five from lineage 5B and three from lineage 21A. **(B)** Combined connectivity per hemilineage, cumulative count of synapses between GF dendrites and hemilineage neurons. The connectivity between hemilineage 8B and the GF is significant, spanning 339 synapses. Hemilineage 7B, 5B and 21A forms 45, 205 and 108 connections, respectively. **(C)** Weighted connectivity per hemilineage, calculated as the cumulative count of synapses between GF dendrites and hemilineage neurons, divided by the total number of GF output connections observed at a threshold of five synapses per neuron. Hemilineage 8B contributes heavily, making up 25% of GF input, followed by 15% from lineage 5B. Lineage 7B contributes 3.3% and lineage 21A 8%. **(D)** Count of neurons per hemilineage that form synapses with GF axons. A total of 13 hemilineages are downstream synaptic partners of the GF. Of those, the synapses formed with lineage 8B are most divergent and span 12 neurons. **(E)** Combined connectivity per hemilineage, cumulative

count of synapses between GF axons and hemilineage neurons. Hemilineage 8B makes 208 synaptic contacts. Hemilineage 18B and 6B also form strong connections, 206 and 121 connections, albeit with fewer neurons (5 and 6, respectively). **(F)** Weighted connectivity per hemilineage, calculated as the cumulative count of synapses between GF axons and hemilineage neurons, divided by the total number of GF output connections observed at a threshold of five synapses per neuron. 12.5% of output GF synaptic contacts are made with hemilineage 8B, followed by 12.4 % with lineage 18B and 7.3% with lineage 6B.

Video legends:

Video-1A-1	hemilineage 1A activation on a decapitated animal, 60 frame per second (FPS)
Video-1A-2	hemilineage 1A activation on an intact animal, 50FPS
Video-1B-1	hemilineage 1B activation on a decapitated animal, 40FPS
Video-1B-2	hemilineage 1B activation on an intact animal, 40FPS
Video-2A-1	hemilineage 2A activation on a decapitated animal, 60FPS
Video-2A-2	hemilineage 2A activation on an intact animal, 40FPS
Video-4B-1	hemilineage 4B activation on a decapitated animal, 72FPS
Video-4B-2	hemilineage 4B activation on an intact animal, 72FPS
Video-5B-1	hemilineage 5B activation on a decapitated animal, 60FPS
Video-5B-2	hemilineage 5B activation on an intact animal, 50FPS
Video-5B-3	hemilineage 5B activation on an intact feeding animal, 25FPS
Video-5B-4	hemilineage 5B activation on an intact animal-tethered flight, 25FPS
Video-5B-5	hemilineage 5B activation on an intact animal walking, 25FPS
Video-6B-1	hemilineage 6B activation on a decapitated animal, 40FPS
Video-6B-2	hemilineage 5B activation on an intact animal-tethered flight, 81FPS
Video-7B-1	hemilineage 7B activation on a decapitated animal, 40FPS
Video-7B-2	hemilineage 7B activation on a decapitated animal, 500FPS-5Xslower
Video-7B-3	hemilineage 7B activation on an intact animal, 40FPS
Video-8A-1	hemilineage 8A activation on a decapitated animal, 40FPS
Video-8A-2	hemilineage 8A activation on an intact animal, 40FPS
Video-8B-1	hemilineage 8B activation on a decapitated animal, 500FPS-10Xslower
Video-8B-2	hemilineage 8B activation on an intact animal, 500FPS-10Xslower
Video-9A-1	hemilineage 9A activation on a tethered decapitated animal, 40FPS
Video-9A-2	hemilineage 9A activation on a decapitated animal, 40FPS

Video-9A-3 hemilineage 9A activation on an intact animal, 40FPS

Video-9B-1 hemilineage 9B activation on a decapitated animal, 40FPS

Video-9B-2 hemilineage 9B activation on an intact animal, 40FPS

Video-10B-1 hemilineage 10B activation on a decapitated animal, 60FPS

Video-10B-2 hemilineage 10B activation on an intact animal, 50FPS

Video-11A-1 hemilineage 11A activation with a strong stimulation on a decapitated animal, 500FPS-10Xslower

Video-11A-2 hemilineage 11A activation with a weak stimulation on a decapitated animal, 500FPS

Video-11A-3 hemilineage 11A activation with a strong stimulation on an intact animal, 40FPS

Video-11A-4 hemilineage 11A activation with a weak stimulation on an intact animal, 40FPS

Video-11B-1 hemilineage 11B activation on a decapitated animal, 40FPS

Video-11B-2 hemilineage 11B activation on an intact animal, 40FPS

Video-12A-1 T1 clonal activation of hemilineage 12A neurons on a decapitated animal, sample 1, 100FPS

Video-12A-2 T1 clonal activation of hemilineage 12A neurons on a decapitated animal, sample 2, 100FPS

Video-13A-1 hemilineage 13A activation on a decapitated animal, 40FPS

Video-13A-2 hemilineage 13A activation on two intact animals, 40FPS

Video-13B-1 hemilineage 13B activation on a decapitated animal, 40FPS

Video-13B-2 hemilineage 13B activation on an intact animal, 40FPS

Video-14A-1 hemilineage 14A activation on a decapitated animal, 60FPS

Video-14A-2 hemilineage 14A activation on an intact animal, 40FPS

Video-15B-1 hemilineage 15B activation on a decapitated animal, 50FPS

Video-15B-2 hemilineage 15B activation on an intact animal, 40FPS

Video-16B-1 hemilineage 16B activation on a decapitated animal, 60FPS

Video-16B-2 hemilineage 16B activation on an intact animal, 40FPS

Video-17A-1 hemilineage 17A activation on a decapitated animal, 40FPS

Video-17A-2 hemilineage 17A activation on an intact animal, 40FPS

Video-19A-1 hemilineage 19A activation on a decapitated animal, 40FPS

Video-19A-2 hemilineage 19A activation on an intact animal, 40FPS

Video-21A-1 hemilineage 21A activation on a decapitated animal, 25FPS

Video-21A-2 hemilineage 21A activation on an intact tethered animal, 200FPS

Video-23B-1 hemilineage 23B activation on a decapitated animal, 33FPS

Video-23B-2 hemilineage 23B activation on an intact animal, 47FPS

Supplementary Table Legends

Supplementary Table 1: Detailed description of the expression patterns of the driver lines used in Figure 3 and Figure 3 Supplemental Figure 1.

Supplementary Table 2: Synaptic inputs of the Giant Fiber neuron related to Figure 6.

Supplementary Table 3: Synaptic outputs of the Giant Fiber neuron related to Figure 6.

Supplementary Table 4: Additional information on CRISPR genomic edits.

Supplementary Table 5: Genotypes of animals used for each figure and video

Table 1: Overview of cluster annotation, lineage specific marker genes and tested split-GAL4 driver lines.

Lineage	Clusters (Allen et al.)	Markers	Driver line Combinations
0A	22, 88, 112	En, Inv, Fkh, Tj, Lim1, grn, HLH3B, Mab-21, Gad1	inv-GAL4-DBD, tj-p65.AD: * * * * fkh-GAL4-DBD, tj-p65.AD: * * * * mab21-p65.AD, fkhGAL4-DBD: * * *
1A	16	Dr, Ets21C, Ptx1, ChAT	Dr-p65.AD, ets21C-GAL4-DBD: * * *
1B	12, 47	HLH4C, H15, Mid, Gad1	HLH4C-GAL4-DBD, H15-p65.AD: * * *
2A	15, 86	HLH3B, Oc, Sox21a, Drgx, Lim1, grn, svp, VGlut	sox21a-GAL4-DBD, VGlut-p65.AD: * * * * sox21a-GAL4-DBD, lim1-VP16.AD: * * *
3A	7, 37, 85	H15, HGTX, Grn, Lim1, ChAT	H15-p65.AD, ChaT-GAL4-DBD: *
3B	26	Fer3, CG4328, Gad1	fer3-GAL4-DBD, cg4328-p65.AD: *
4B	0, 100	Exex, Ap, Fkh, Tey, HGTX, HLH4C, Oc, ChAT	ap-p65.AD, fkhGAL4-DBD: * * * ap-p65.AD, hgtx-GAL4-DBD: * * * *
5B	20, 87, 97	Vg, Toy, Vsx2, Lim1, Gad1	vg-p65.AD, toy-GAL4-DBD: * * * *
6A	9, 28	Mab-21, Toy, Gad1	mab21-p65.AD, toy-GAL4-DBD: * *
6B	3, 89	Vg, Sens-2, En, CG4328, Vsx2, Gad1	sens2-p65.AD, vg-GAL4-DBD sens2-GAL4-DBD, vg-p65.AD: * * CG4328-p65.AD, vg-GAL4-DBD: * * *
7B	2, 62	Unc-4, Sv, Mab-21, ChAT	unc-4-p65.AD, mab21-GAL4-DBD: * * * unc-4-GAL4-DBD, sv-p65.AD: * * *

8A	6, 69, 110	Ey, Ems, Toy, Ets65A, VGluT	ems-GAL4-DBD, eyAD: * * * * ems-GAL4-DBD, toy-p65.AD: * * ems-GAL4-DBD, vGluT-p65.AD: * * *
8B	8, 53, 76	C15, Lim3, Acj6, ChAT	C15-p65.AD, lim3-GAL4-DBD: * * *
9A	31, 50, 56, 57	Dr, Ets65A, grn, sox21a, Gad1	Dr-p65.AD, gad1-GAL4-DBD: * * * * Dr-p65.AD, sox21a-GAL4-DBD: * * * *
9B	54, 76	Lim3, Drgx, Sens-2, Acj6, Tup, HLH4C, VGluT	acj6-p65.AD, VGluT-GAL4-DBD: * * *
10B	39, 68, 91	Exex, Kn, Sens-2, Lim3, ChAT	knot-p65.AD, hb9-GAL4-DBD: * * * * hb9-p65.AD, sens-2-GAL4-DBD: * * * * knot-p65.AD, nkx6-GAL4-DBD: * * * * knot-p65.AD, lim3-GAL4-DBD: * * *
11A	21	Unc-4, Tey, ChAT	unc-4-GAL4-DBD, tey-VP16: * * * unc-4-p65.AD, hgtx-GAL4-DBD: * * *
11B	38	Eve, HLH4C, Gad1	eve-p65.AD, gad1-GAL4-DBD: * * * *
12A	40	Unc-4, TfAP-2, Grn, ChAT	unc-4-GAL4-DBD, TfAP2-p65.AD: * * *
12B	30, 73, 81, 83, 94	Fer3, HGTX, CG4328, H15, Tey, Gad1	HGTX-GAL4-DBD, gad1-p65.AD: * *
13A	48, 75, 79	Dbx, Fer2, Dmrt99B, Gad1	dbx-GAL4-DBD, dmrt99B-p65.AD: * *
13B	17 , 25	D, Vg, CG4328, tey, svp, Gad1	vg-GAL4-DBD, D-VP16.AD: * * vg-GAL4-DBD, tey-VP16.AD: * * *
14A	13, 41, 74	Dr, Toy, Lim1, Ets65A, Grn, VGluT,	Dr-p65.AD, toy-GAL4-DBD: * * *
15B	36, 52, 80	Tup, Lim3, HGTX, VGlut	HGTX-GAL4-DBD, VGlut-p65.AD: * * * nkx6- GAL4-DBD, twit-p65.AD: * * *
16B	5, 46	Lim3, Exex, Bi, Sp1, VGlut,	hb9-p65.AD, bi-GAL4-DBD: * * * hb9-p65.AD, VGlut-GAL4-DBD: * * *
17A	58, 77	Unc-4, Hmx, Tup, ChAT	unc-p65.AD, hmx-GAL4-DBD: * * * *
18B	N/A	Unc-4, ChAT	**No line**
19A	19, 59, 82	Dbx, Fer2, Scro, Gad1	dbx-GAL4-DBD, scro-p65.AD: * * *
19B	27, 71	Unc-4, Otp, ChAT	**No line**
20/22A	14, 33, 34, 78, 108	Bi, Ets65A, Sv, ChAT	sv-p65.AD, ets65-GAL4-DBD: * * * bi-GAL4-DBD, shaven-p65.AD: * * bi-p65.AD, ets65A-GAL4-DBD: * *
21A	1	Dr, Ey, Tj, VGluT	Dr-p65.AD, tj-GAL4-DBD: * * * * Dr-p65.AD, ey-GAL4-DBD: * * *
23B	35, 51, 67, 93	Unc-4, Acj6, Slou, Otp, ChAT	unc-4-p65.AD, acj6-GAL4-DBD: * * *
24B	A small subset of	Toy, Ems, Twit, VGlut	ems-GAL4-DBD, twit-p65.AD: * * *

	clusters 52 and 36		

**** Very specific for one hemilineage; *** Specific, some contamination from other neurons; ** Somewhat specific, significant contribution of e.g. motor neurons or sensory neurons; * More than one hemilineage marked

Table 2: Overview of behavioral phenotypes upon optogenetic activation of specific hemilineages.

Lineage	***Genotype*: Phenotype**	**Videos**
0A	*tj-p65.AD, inv-GAL4-DBD*: No apparent behavioral response observed in response to acute optogenetic activation.	N/A
1A	*Dr-p65.AD, Ets21C-GAL4-DBD*: Activation in both intact and decapitated animals drove leg extension making fly taller. Our observation differed from previously observed phenotypes of erratic forward locomotion, occasionally interrupted by grooming in decapitated animals (Harris et al., 2015).	Video-1A-1; Video-1A-2
1B	*H15-p65.AD, HLH4C-GAL4-DBD*: Activation in both intact and decapitated flies drives leg rotational movement causing the joint between the femur and tibia to bend laterally, most pronounced by the hind legs.	Video-1B-1; Video-1B-2
2A	*VGlut-p65.AD, Sox21a-GAL4-DBD*: Activation in intact animals drove high-frequency wing flapping, consistent with the findings of Harris et al which showed the same phenotype with the decapitated flies. In our experiments with decapitated animals, no wing buzzing was observed, and only halteres moved ventrally upon stimulation.	Video-2A-1; Video-2A-2
4B	*ap-p65.AD, HGTX-GAL4-DBD*: Activation cause a full extension of all the legs in both decapitated and intact flies.	Video-4B-1; Video-4B-2
5B	*vg-p65.AD, toy-GAL4-DBD*: Activation of 5B neurons halts almost every movement in the animal, causing walking, grooming, flying (tethered flight assay), and feeding flies to halt these behaviors. Decapitated animals also halt their grooming activity in response to 5B activation. Active 5B neurons also halt the larval locomotion.	Video-5B-1; Video-5B-2; Video-5B-3; Video-5B-4
6B	*CG4328-p65.AD, vg-GAL4-DBD*: Activation in intact animals drove inhibition in wing buzzing and leg movements of the tethered flies. Activation in decapitated animals halted sporadic leg movements and drove a subtle change in the posture.	Video-6B-1; Video-6B-2
7B	*sv-p65.AD, unc-4-GAL4-DBD*: Upon 7B activation, both decapitated and intact animals raised their wings and attempted to takeoffs, but only a few showed modest take-off behavior. We also observed tibia levitation in response to activation. Harris et al. observed robust take off behavior.	Video-7B-1; Video-7B-2; Video-7B-3
8A	*ey-p65.AD, ems-GAL4-DBD*: Activation brings the body of the fly closer to the ground likely flexing leg segments in both intact and decapitated animals. Harris et al. observed minimal effects after activation.	Video-8A-1; Video-8A-2
8B	*C15-p65.AD, Lim3-GAL4-DBD*: Activation drove intact animals lean backward and take-off. A few animals initiated wing flapping after the jump; others failed to initiate wing flapping and fall after the jump, then they jumped again under the continuous activation. Decapitated animals showed a similar response but never initiated the wing flapping after the take-off.	Video-8B-1; Video-8B-2

9A	*Dr-p65.AD, Gad1-GAL4-DBD*: Activation in intact animals drove erratic forward locomotion of the animal. Activation in tethered intact flies restricted the legs to stay in a specific posture. In decapitated animals, bodies were lowered toward the ground with legs becoming more splayed for approximately two seconds before occasional forward locomotion and leg grooming, consistent with previous research by Harris et al.	Video-9A-1; Video-9A-2; Video-9A-3
9B	*acj6-p65.AD, VGlut-GAL4-DBD*: Activation in intact animals did not lead to any robust behavior; occasionally animals changed their posture mildly. Decapitated animals halted their grooming in response to 9B activation. This halting behavior was less penetrant compared to the halting behavior observed with 5B activation.	Video-9B-1; Video-9B-2;
10B	*Hb9-p65-AD, sens-2-GAL4-DBD*: Activation in intact animals drove erratic walking behavior. 10B activation in decapitated animals drove leg extension and body twisting. Our findings differed from Harris et al. 2015, which showed erratic leg movements causing backwards locomotion with occasional wing flicking and buzzing.	Video-10B-1; Video-10B-2;
11A	*tey-VP16.AD, unc-4-GAL-4-DBD*: Low intensity light activation drove lateral wing waving with occasional jumping, while high intensity activation drove wing buzzing and jumping in intact and decapitated animals.	Video-11A-1; Video-11A-2; Video-11A-3; Video-11A-4
11B	*eve-p65.AD, Gad1-GAL4-DBD*: Harris et al., observed take-off behavior after activation of the 11B neurons. However, upon light activation, we observed wing movements without any take-off behavior. The wings moved from side to side in a buzzing behavior.	Video-11B-1; Video-11B-2
12A	*TfAP2-p65.AD, unc-4-GAL4-DBD*: CsChrimson expression showed a lethal phenotype with no surviving adults. We generated linage clones using TfAP-2-GAL4. Animals expressing CsChrimson in 12A neurons in one side of the T1 segment showed a single swing movement of the leg that is located on the same side of the animal lineage clone located. We also observed bilateral wing buzzing.	Video-12A-1; Video-12A-2
13A	*dmrt99B-p.65AD, dbx-GAL4-DBD*: Upon 13A activation, intact flies halt their walking and grooming behaviors, and change the body posture, making flies slightly taller due to likely femur-coxa extension. Decapitated flies also halt the grooming behavior in response to 13A activation. Both intact and decapitated flies buzz their wings in response to activation, a phenotype likely arise from contaminating neurons.	Video-13A-1; Video-13A-2
13B	*D-VP16.AD, vg-GAL4-DBD*: Intact flies lost control of their legs and fell on their back with uncoordinated leg movements upon activation of 13B neurons. Decapitated flies responded with a postural change and a weak leg extension phenotype.	Video-13B-1; Video-13B-2
14A	*Dr-p65.AD, toy-GAL4-DBD*: Activation caused intact animals to fall on their back or side with uncoordinated leg movements; flies remained uncoordinated until the cessation of the stimulus. In decapitated animals, activation drove femur-tibia joint to move anteriorly, most pronounced in the middle legs. We also observed flexion of the legs.	Video-14A-1; Video-14A-2
15B	*VGlut-p65.AD, HGTX-GAL4-DBD*: Upon light stimulation in both intact and decapitated flies, the legs showed a severe flexing phenotype. The legs flexed tightly against the body with the flies falling into a fetal position until after light stimulation ended.	Video-15B-1; Video-15B-2
16B	*Hb9-p65.AD, Bi-GAL4-DBD*: Activation in both intact and decapitated animals drove flexion at the femur-tibia joint and coxa-femur axis joint causing the animal to sink lower to the ground.	Video-16B-1; Video-16B-2

17A	*unc-4-p65.AD, Hmx-GAL4-DBD*: Activation of 17A neurons drove flexion of all the leg segments in both decapitated and intact animals.	Video-17A-1; Video-17A-2
19A	*scro-p65.AD, dbx-GAL4-DBD*: Activation in decapitated animals drove flexion at the tibia-tarsus joint as well as anterior movement of the femur-tibia axis. In intact animals, we observed severe flexing of the legs against the body making flies to fall on their back. Harris et al., observed a leg-waving phenotype of the T2 legs in decapitated animals after stimulation.	Video-19A-1; Video-19A-2
21A	*Dr-p65.AD, tj-GAL4-DBD*: Activation of 21A neurons in decapitated animals drove flexion of the legs bringing the body of the fly closer to the ground. We observed a similar phenotype in intact animals tethered to a pin.	Video-21A-1; Video-21A-2
23B	*unc-4-p65.AD, acj6-GAL4-DBD*: Activation caused intact animals to fall on their back due to uncoordinated leg movements and sustained flexion or extension of the leg segments; flies remained uncoordinated until the cessation of the stimulus. Flies also showed increased grooming activity. We also observed wing buzzing in response to activation. Decapitated animals showed similar responses.	Video-23B-1; Video-23B-2

Key Resources Table

Reagent type (species or resource)	Designation	Source	Identifier	Additional Information
Antibody	guinea pig anti-tj polyclonal	Gift from Dorothea Godt		1:5000 dilution
Antibody	Rabbit anti-tey polyclonal	Gift from Angelike Stathopoulos		1:200 dilution
Antibody	Rat anti-c15 polyclonal	Gift from Gerard Campbell		1:1000 dilution
Antibody	Chicken anti-GFP polyclonal	Life Technologies	A-10262	1:1000 dilution
Antibody	Rabbit anti-GFP polyclonal	Life Technologies	A-11122	1:1000 dilution
Antibody	Rabbit anti-Unc-4 polyclonal	Lacin et al., 2014	A-10262	1:1000 dilution
Antibody	Mouse anti-Acj6 monoclonal	DSHB	Acj6	1:100 dilution
Antibody	Rat anti-CadN monoclonal	DSHB	DN-Ex #8	1:25 dilution
Antibody	Mouse anti-Neuroglian monoclonal	DSHB	BP104	1:25 dilution
Antibody	Goat anti-rabbit Alexa Fluor 488	Life Technologies	A-11034	1:500 dilution
Antibody	Goat anti-rabbit Alexa Fluor 568	Life Technologies	A-11011	1:500 dilution
Antibody	Goat anti-rabbit Alexa Fluor 633	Life Technologies	A-21070	1:500 dilution
Antibody	Goat anti-rat Alexa Fluor 633	Life Technologies	A-21094	1:500 dilution
Antibody	Goat anti-chicken Alexa Fluor 488	Life Technologies	A-11039	1:500 dilution
Antibody	Goat anti-mouse Alexa Fluor 568	Life Technologies	A-11001	1:500 dilution
Antibody	Goat anti-mouse Alexa Fluor 633	Life Technologies	A-21050	1:500 dilution
Antibody	Goat anti-rat Alexa Fluor 568	Life Technologies	A-21050	1:500 dilution

Genetic reagent (*D. melanogaster*)	unc-4DBD/FM7GFP; 20XUASCsChrimson_attp40/cyo	Lacin et al.,2020		
Genetic reagent (*D. melanogaster*)	unc-4AD/FM7; 20X-UASChrimson_attp40/cyo	Lacin et al.,2020		
Genetic reagent (*D. melanogaster*)	sens2-GAL4-DBD	Lacin et al., 2024		
Genetic reagent (*D. melanogaster*)	P{w[+mW.hs]=GawB}elav[C155]; P{w[+mW.hs]=FRT(w[hs])}G13 P{w[+mC]=tubP-GAL80}LL2	Tzumin Lee Lab		
Genetic reagent (*D. melanogaster*)	20XUAS-CsChrimson-mVenus_attp18	V. Jayaraman lab		
Genetic reagent (*D. melanogaster*)	20XUAS>FRT-stop>CsChrimson-mVenus_attp18	V. Jayaraman lab		
Genetic reagent (*D. melanogaster*)	P{GawB}elav[C155], P{FRT(w[hs])}G13 P{UAS-mCD8::GFP.L}LL5	Tzumin Lee Lab		
Genetic reagent (*D. melanogaster*)	P{FRT(w[hs])}G13 P{tubP-GAL80}LL2	Tzumin Lee Lab		
Genetic reagent (*D. melanogaster*)	y[1] w1118; P{tubP-GAL80}LL9 P{FRT(w[hs])}2A/TM3, Sb	Tzumin Lee Lab		
Genetic reagent (*D. melanogaster*)	knot-p65.AD/CyO, weep; Dr/TM6	Luo Lab, Hongjie Li		
Genetic reagent (*D. melanogaster*)	pin/cyo; c15-p65.AD/TM6b	Luo Lab, Hongjie Li		
Genetic reagent (*D. melanogaster*)	tj-vp16.AD	Desplan Lab-David Chen		
Genetic reagent (*D. melanogaster*)	twit-p65.AD	Stephen Goodwin		
Genetic reagent (*D. melanogaster*)	13XLexAop2-IVS-myr::GFP in attP40	BDSC	RRID:BDSC 32210	
Genetic reagent (*D. melanogaster*)	P{hsFLP}1; P{FRT(w[hs])}G13 P{tubP-GAL80}LL2/CyO	BDSC	RRID:BDSC 5145	
Genetic reagent (*D. melanogaster*)	P{tubP-GAL80}LL10 P{neoFRT}40A/CyO	BDSC	RRID:BDSC 5192	
Genetic reagent (*D. melanogaster*)	w[*]; l(2)*[*]/CyO; Mi{Trojan-GAL4DBD.0}ChAT[MI04508-TG4DBD.0] CG7715[MI04508-TG4DBD.0-X]/TM3, Sb[1]	BDSC	RRID:BDSC 60318	
Genetic reagent (*D. melanogaster*)	w1118; PBac{RB}Fer2e03248	BDSC	RRID:BDSC 26028	
Genetic reagent (*D. melanogaster*)	w1118; PBac{Sp1-EGFP.S}VK00033	BDSC	RRID:BDSC 38669	
Genetic reagent (*D. melanogaster*)	w[1118]; PBac{y[+mDint2] w[+mC]=fkh-GFP.FPTB}VK00037/SM5	BDSC	RRID:BDSC 43951	

Genetic reagent (*D. melanogaster*)	y[1] w[*]; Mi{y[+mDint2]=MIC}twit[MI06552]/(SM6a)	BDSC	RRID:BDSC 41449	
Genetic reagent (*D. melanogaster*)	w[*]; Mi{Trojan-GAL4DBD.0}Dbx[MI05316-TG4DBD.0]/TM6B, Tb[1]	Lacin et al., 2019	RRID:BDSC 82989	
Genetic reagent (*D. melanogaster*)	y[1] w[*]; Mi{Trojan-GAL4DBD.1}Lim3[MI03817-TG4DBD.1]/(CyO)	Lacin et al., 2019	RRID:BDSC 82990	
Genetic reagent (*D. melanogaster*)	w1118; PBac{WH}Ets21Cf03639	BDSC	RRID:BDSC 18678	
Genetic reagent (*D. melanogaster*)	w[*]; Mi{Trojan-p65AD.2}VGlut[MI04979-Tp65AD.2]/CyO	Lacin et al., 2019	RRID:BDSC 82986	
Genetic reagent (*D. melanogaster*)	w[*]; betaTub60D[Pin-1]/CyO; Mi{Trojan-p65AD.1}Dr[MI14348-Tp65AD.1]	Lacin et al., 2019	RRID:BDSC 82991	
Genetic reagent (*D. melanogaster*)	y[1] w[*]; Mi{y[+mDint2]=MIC}Dr[MI14348]/TM3, Sb[1] Ser[1]	BDSC	RRID:BDSC 59504	
Genetic reagent (*D. melanogaster*)	w[*]; betaTub60D[Pin-1]/CyO; TI{2A-GAL4(DBD)::Zip-}HGTX[DBD]/TM6B, Tb[1]	Lacin et al., 2019	RRID:BDSC 82992	
Genetic reagent (*D. melanogaster*)	ey-GAL4-DBD	Lacin et al., 2019	RRID:BDSC 6294	
Genetic reagent (*D. melanogaster*)	y[1] w[*]; Mi{y[+mDint2]=MIC}Ets65A[MI05707]	BDSC	RRID:BDSC 40235	
Genetic reagent (*D. melanogaster*)	y[1] w[*]; TI{GFP[3xP3.cLa]=CRIMIC.TG4.2}sv[CR00370-TG4.2]	BDSC	RRID:BDSC 78901	
Genetic reagent (*D. melanogaster*)	y[1] w[*]; TI{GFP[3xP3.cLa]=CRIMIC.TG4.2}Sox21a[CR00451-TG4.2]/TM3 Sb[1] Ser[1]	BDSC	RRID:BDSC 83174	
Genetic reagent (*D. melanogaster*)	y[1] w[*] Mi{y[+mDint2]=MIC}bi[MI08152] lncRNA:CR32773[MI08152]	BDSC	RRID:BDSC 51220	
Genetic reagent (*D. melanogaster*)	y[1] w[*]; Mi{y[+mDint2]=MIC}ap[MI01996]/CyO	BDSC	RRID:BDSC 42297	
Genetic reagent (*D. melanogaster*)	y[1] w[*]; Mi{y[+mDint2]=MIC}inv[MI09433]	BDSC	RRID:BDSC 52163	
Genetic reagent (*D. melanogaster*)	y[1] w[*] Mi{y[+mDint2]=MIC}acj6[MI07818]	BDSC	RRID:BDSC 51212	
Genetic reagent (*D. melanogaster*)	y[1] w[*]; Mi{PT-GFSTF.2}Hmx[MI02025-GFSTF.2]/TM3, Sb[1] Ser[1]	BDSC	RRID:BDSC 59785	

Genetic reagent (*D. melanogaster*)	y[1] w[*]; Mi{y[+mDint2]=MIC}Hmx[MI02896]	BDSC	RRID:BDSC 36161	
Genetic reagent (*D. melanogaster*)	y[1] w[*]; Mi{y[+mDint2]=MIC}Ets65A[MI05707]	BDSC	RRID:BDSC 40235	
Genetic reagent (*D. melanogaster*)	y[1]; Mi{y[+mDint2]=MIC}toy[MI03240]	BDSC	RRID:BDSC 61701	
Genetic reagent (*D. melanogaster*)	P{Tub-dVP16AD.D}	BDSC	RRID:BDSC 60295	
Genetic reagent (*D. melanogaster*)	P{Tub-GAL4DBD.D}	BDSC	RRID:BDSC 60298	
Genetic reagent (*D. melanogaster*)	lim3-GAL4-DBD	Lacin et al., 2019	RRID:BDSC 82990	
Genetic reagent (*D. melanogaster*)	ChAT-p65.AD	Lacin lab		RMCE with RRID:BDSC37817
Genetic reagent (*D. melanogaster*)	y[*]w[*]/w[*];inv[MI09433.p65AD_1]/SM6a	generated in this study		RMCE with RRID:BDSC 52163
Genetic reagent (*D. melanogaster*)	ap-GAL4-DBD	generated in this study		RMCE with RRID:BDSC 42297
Genetic reagent (*D. melanogaster*)	ap-p65.AD	generated in this study		RMCE with RRID:BDSC 42297
Genetic reagent (*D. melanogaster*)	mab-21-GAL4-DBD	generated in this study		RMCE with RRID:BDSC 59220
Genetic reagent (*D. melanogaster*)	mab-21-p65.AD	generated in this study		RMCE with RRID:BDSC 59220
Genetic reagent (*D. melanogaster*)	toy-GAL4-DBD	generated in this study		RMCE with RRID:BDSC 61701
Genetic reagent (*D. melanogaster*)	toy-p65.AD	generated in this study		RMCE with RRID:BDSC 61701
Genetic reagent (*D. melanogaster*)	shaven-p65.AD	generated in this study		RMCE with RRID:BDSC 78901
Genetic reagent (*D. melanogaster*)	sox21a-GAL4-DBD	generated in this study		RMCE with RRID:BDSC 93174
Genetic reagent (*D. melanogaster*)	bi-GAL4-DBD	generated in this study		RMCE with RRID:BDSC 51220
Genetic reagent (*D. melanogaster*)	bi-p65.AD	generated in this study		RMCE with RRID:BDSC 51220

Genetic reagent (*D. melanogaster*)	CG4328-p65.AD	generated in this study		RMCE with RRID:BDSC 42307
Genetic reagent (*D. melanogaster*)	Ets65A-GAL4-DBD	generated in this study		RMCE with RRID:BDSC 56352
Genetic reagent (*D. melanogaster*)	Hmx-GAL4-DBD	generated in this study		RMCE with RRID:BDSC 36161
Genetic reagent (*D. melanogaster*)	dmrt99b-GAL4-DBD	generated in this study		RMCE with RRID:BDSC 92707
Genetic reagent (*D. melanogaster*)	dmrt99b-p65.AD	generated in this study		RMCE with RRID:BDSC 92707
Genetic reagent (*D. melanogaster*)	Dr-GAL4-DBD	generated in this study		RMCE with RRID:BDSC 59504
Genetic reagent (*D. melanogaster*)	exex-GAL4-DBD	generated in this study		RMCE with exex-p65AD[attP2FRT2]
Genetic reagent (*D. melanogaster*)	vg-GAL4-DBD	generated in this study		RMCE with vg-p65AD[attP2FRT2]
Genetic reagent (D. melanogaster)	sens2-p65.AD	generated in this study		RMCE with sens2-GAL4-DBD[attP2FRT2]
Genetic reagent (*D. melanogaster*)	Ets21C-GAL4-DBD	generated in this study		RMCE with Ets21C-p65.AD[attP2FRT2]
Genetic reagent (*D. melanogaster*)	eve-GAL4-DBD	generated in this study		RMCE with eve-p65.AD[attP2FRT2]
Genetic reagent (*D. melanogaster*)	exex-p65.AD[attP2FRT2]	generated in this study		CRISPR /Trojan (CRIMIC)
Genetic reagent (*D. melanogaster*)	exex-GAL4-DBD[attP2FRT2]	generated in this study		CRISPR /Trojan (CRIMIC)
Genetic reagent (*D. melanogaster*)	eve-p65.AD[attP2FRT2]	generated in this study		CRISPR /Trojan (CRIMIC)
Genetic reagent (*D. melanogaster*)	vg-p65.AD[attP2FRT2]	generated in this study		CRISPR /Trojan (CRIMIC)
Genetic reagent (*D. melanogaster*)	vg-GAL4-DBD[attP2FRT2]	generated in this study		CRISPR /Trojan (CRIMIC)

Genetic reagent (*D. melanogaster*)	H15-p65.AD[attP2FRT2]	generated in this study		CRISPR /Trojan (CRIMIC)
Genetic reagent (*D. melanogaster*)	scro-p65.AD[attP2FRT2]	generated in this study		CRISPR /Trojan (CRIMIC)
Genetic reagent (*D. melanogaster*)	scro-GAL4-DBD[attP2FRT2]	generated in this study		CRISPR /Trojan (CRIMIC)
Genetic reagent (*D. melanogaster*)	Ets21C-p65.AD[attP2FRT2]	generated in this study		CRISPR /Trojan (CRIMIC)
Genetic reagent (*D. melanogaster*)	Ets21C-GAL4-DBD[attP2FRT2]	generated in this study		CRISPR /Trojan (CRIMIC)
Genetic reagent (*D. melanogaster*)	eve-p65.AD[attP2FRT2]	generated in this study		CRISPR /Trojan (CRIMIC)
Genetic reagent (*D. melanogaster*)	Fer3-GAL4-DBD	generated in this study		CRISPR /In frame insertion (C terminus)
Genetic reagent (*D. melanogaster*)	ems-GAL4-DBD	generated in this study		CRISPR /In frame insertion (C terminus)
Genetic reagent (*D. melanogaster*)	HLH4C-GAL4-DBD	generated in this study		CRISPR /In frame insertion (2nd exon)
Genetic reagent (*D. melanogaster*)	w1118;; fkh-T2A-GAL4-DBD/TM6b	generated in this study by Erclik Lab		CRISPR /In frame insertion (C terminus for RA isoform)
Genetic reagent (*D. melanogaster*)	w*;; D-VP16/TM6b	generated in this study by Erclik Lab		CRISPR /In frame insertion (C terminus)
Genetic reagent (*D. melanogaster*)	pJFRC29-10XUAS-IVS-myr::GFP-p10 in attP40 or attP2	Rubin Lab		-
Genetic reagent (*D. melanogaster*)	pJFRC105-10XUAS-IVS-nlstdTomato in VK0003	Rubin Lab		-
Genetic reagent (*D. melanogater*)	pJFRC12-10XUAS-IVS-myr::GFP attp40 or attP2	Rubin Lab		
Genetic reagent (*D. melanogater*)	pJFRC28-10XUAS-IVS-GFP-p10 in attP2	Rubin Lab		
Chemical compound, drug	Paraformaldehyde	EMS	15713	
Chemical compound, drug	Vectashield	Vectorlabs	H-1000	
Chemical compound, drug	DPX	Electron Microscopy Sciences	50980370	
Chemical compound, drug	Gibson Assembly® Master Mix	New England Biolabs	E2621S	
Recombinant DNA reagent	pCFD4-U6:1_U6:3tandemgRNAs	Addgene	49411	

Recombinant DNA reagent	pBS-KS-attB2-SA(1)-T2A-Gal4-Hsp70	Addgene	62897	
Recombinant DNA reagent	pBS-KS-attB2-SA(1)-T2A-Gal4DBD-Hsp70	Addgene	62903	
Recombinant DNA reagent	pBS-KS-attB2-SA(1)-T2A-p65AD-Hsp70	Addgene	62914	
Recombinant DNA reagent	pBS-KS-attB2-SA(0)-T2A-Gal4-Hsp70	Addgene	62896	
Recombinant DNA reagent	pBS-KS-attB2-SA(0)-T2A-Gal4DBD-Hsp70	Addgene	62902	
Recombinant DNA reagent	pBS-KS-attB2-SA(0)-T2A-p65AD-Hsp70	Addgene	62912	
Recombinant DNA reagent	pBS-KS-attP2FRT2-SA(0)-T2A-p65AD-Hsp70	generated in this study		
Recombinant DNA reagent	pBS-KS-attP2FRT2-SA(1)-T2A-p65AD-Hsp70	generated in this study		
Recombinant DNA reagent	pBS-KS-attP2FRT2-SA(2)-T2A-p65AD-Hsp70	generated in this study		
Recombinant DNA reagent	pBS-KS-attP2FRT2-SA(0)-T2A-gal4DBD-Hsp70	generated in this study		
Recombinant DNA reagent	pBS-KS-attP2FRT2-SA(1)-T2A-gal4DBD-Hsp70	generated in this study		
Recombinant DNA reagent	pBS-KS-attP2FRT2-SA(2)-T2A-gal4DBD-Hsp70	generated in this study		
Recombinant DNA reagent	pCFD4-exex	generated in this study		
Recombinant DNA reagent	pCFD4-vg	generated in this study		
Recombinant DNA reagent	pCFD4-H15	generated in this study		
Recombinant DNA reagent	pUC57_Hb9	generated in this study		
Recombinant DNA reagent	pUC57_vg	generated in this study		
Recombinant DNA reagent	pUC57_H15	generated in this study		
Recombinant DNA reagent	pUC57_gw_OK2_Scro	generated in this study		
Recombinant DNA reagent	pUC57_gw_OK2_Ets21C	generated in this study		
Recombinant DNA reagent	pUC57_gw_OK2_eve	generated in this study		
Recombinant DNA reagent	pUC57_gw_OK2_Fer3	generated in this study		

Recombinant DNA reagent	pUC57_gw_OK2_ems	generated in this study		
Recombinant DNA reagent	pUC57_gw_OK2_HLH4C	generated in this study		

947

Reagent type (species or resource)	Designation	Source	Identifier	Additional Information
Antibody	guinea pig anti-tj polyclonal	Gift from Dorothea Godt		1:5000 dilution
Antibody	Rabbit anti-tey polyclonal	Gift from Angelike Stathopoulos		1:200 dilution
Antibody	Rat anti-c15 polyclonal	Gift from Gerard Campbell		1:1000 dilution
Antibody	Chicken anti-GFP polyclonal	Life Technologies	A-10262	1:1000 dilution
Antibody	Rabbit anti-GFP polyclonal	Life Technologies	A-11122	1:1000 dilution
Antibody	Rabbit anti-Unc-4 polyclonal	Lacin et al., 2014	A-10262	1:1000 dilution
Antibody	Mouse anti-Acj6 monoclonal	DSHB	Acj6	1:100 dilution
Antibody	Rat anti-CadN monoclonal	DSHB	DN-Ex #8	1:25 dilution
Antibody	Mouse anti-Neuroglian monoclonal	DSHB	BP104	1:25 dilution
Antibody	Goat anti-rabbit Alexa Fluor 488	Life Technologies	A-11034	1:500 dilution
Antibody	Goat anti-rabbit Alexa Fluor 568	Life Technologies	A-11011	1:500 dilution
Antibody	Goat anti-rabbit Alexa Fluor 633	Life Technologies	A-21070	1:500 dilution
Antibody	Goat anti-rat Alexa Fluor 633	Life Technologies	A-21094	1:500 dilution
Antibody	Goat anti-chicken Alexa Fluor 488	Life Technologies	A-11039	1:500 dilution
Antibody	Goat anti-mouse Alexa Fluor 568	Life Technologies	A-11001	1:500 dilution
Antibody	Goat anti-mouse Alexa Fluor 633	Life Technologies	A-21050	1:500 dilution
Antibody	Goat anti-rat Alexa Fluor 568	Life Technologies	A-21050	1:500 dilution
Genetic reagent (*D. melanogaster*)	unc-4DBD/FM7GFP; 20XUASCsChrimson_attp40/cyo	Lacin et al.,2020		
Genetic reagent (*D. melanogaster*)	unc-4AD/FM7; 20X-UASChrimson_attp40/cyo	Lacin et al.,2020		
Genetic reagent (*D. melanogaster*)	sens2-GAL4-DBD	Lacin et al., 2024		
Genetic reagent (*D. melanogaster*)	P{w[+mW.hs]=GawB}elav[C155]; P{w[+mW.hs]=FRT(w[hs])}G13 P{w[+mC]=tubP-GAL80}LL2	Tzumin Lee Lab		
Genetic reagent (*D. melanogaster*)	20XUAS-CsChrimson-mVenus_attp18	V. Jayaraman lab		
Genetic reagent (*D. melanogaster*)	20XUAS>FRT-stop>CsChrimson-mVenus_attp18	V. Jayaraman lab		
Genetic reagent (*D. melanogaster*)	P{GawB}elav[C155], P{FRT(w[hs])}G13 P{UAS-mCD8::GFP.L}LL5	Tzumin Lee Lab		
Genetic reagent (*D. melanogaster*)	P{FRT(w[hs])}G13 P{tubP-GAL80}LL2	Tzumin Lee Lab		
Genetic reagent (*D. melanogaster*)	y[1] w1118; P{tubP-GAL80}LL9 P{FRT(w[hs])}2A/TM3, Sb	Tzumin Lee Lab		
Genetic reagent (*D. melanogaster*)	knot-p65.AD/CyO, weep; Dr/TM6	Luo Lab, Hongjie Li		
Genetic reagent (*D. melanogaster*)	pin/cyo; c15-p65.AD/TM6b	Luo Lab, Hongjie Li		

Genetic reagent (*D. melanogaster*)	tj-vp16.AD	Desplan Lab- David Chen		
Genetic reagent (*D. melanogaster*)	twit-p65.AD	Stephen Goodwin		
Genetic reagent (*D. melanogaster*)	13XLexAop2-IVS-myr::GFP in attP40	BDSC	RRID:BDSC 32210	-
Genetic reagent (*D. melanogaster*)	P{hsFLP}1; P{FRT(w[hs])}G13 P{tubP-GAL80}LL2/CyO	BDSC	RRID:BDSC 5145	
Genetic reagent (*D. melanogaster*)	P{tubP-GAL80}LL10 P{neoFRT}40A/CyO	BDSC	RRID:BDSC 5192	
Genetic reagent (*D. melanogaster*)	w[*]; l(2)*[*]/CyO; Mi{Trojan-GAL4DBD.0}ChAT[MI04508-TG4DBD.0] CG7715[MI04508-TG4DBD.0-X]/TM3, Sb[1]	BDSC	RRID:BDSC 60318	
Genetic reagent (*D. melanogaster*)	w1118; PBac{RB}Fer2e03248	BDSC	RRID:BDSC 26028	
Genetic reagent (*D. melanogaster*)	w1118; PBac{Sp1-EGFP.S}VK00033	BDSC	RRID:BDSC 38669	
Genetic reagent (*D. melanogaster*)	w[1118]; PBac{y[+mDint2] w[+mC]=fkh-GFP.FPTB}VK00037/SM5	BDSC	RRID:BDSC 43951	
Genetic reagent (*D. melanogaster*)	y[1] w[*]; Mi{y[+mDint2]=MIC}twit[MI06552]/(SM6a)	BDSC	RRID:BDSC 41449	
Genetic reagent (*D. melanogaster*)	w[*]; Mi{Trojan-GAL4DBD.0}Dbx[MI05316-TG4DBD.0]/TM6B, Tb[1]	Lacin et al., 2019	RRID:BDSC 82989	
Genetic reagent (*D. melanogaster*)	y[1] w[*]; Mi{Trojan-GAL4DBD.1}Lim3[MI03817-TG4DBD.1]/(CyO)	Lacin et al., 2019	RRID:BDSC 82990	
Genetic reagent (*D. melanogaster*)	w1118; PBac{WH}Ets21Cf03639	BDSC	RRID:BDSC 18678	
Genetic reagent (*D. melanogaster*)	w[*]; Mi{Trojan-p65AD.2}VGlut[MI04979-Tp65AD.2]/CyO	Lacin et al., 2019	RRID:BDSC 82986	
Genetic reagent (*D. melanogaster*)	w[*]; betaTub60D[Pin-1]/CyO; Mi{Trojan-p65AD.1}Dr[MI14348-Tp65AD.1]	Lacin et al., 2019	RRID:BDSC 82991	
Genetic reagent (*D. melanogaster*)	y[1] w[*]; Mi{y[+mDint2]=MIC}Dr[MI14348]/TM3, Sb[1] Ser[1]	BDSC	RRID:BDSC 59504	
Genetic reagent (*D. melanogaster*)	w[*]; betaTub60D[Pin-1]/CyO; TI{2A-GAL4(DBD)::Zip-}HGTX[DBD]/TM6B, Tb[1]	Lacin et al., 2019	RRID:BDSC 82992	
Genetic reagent (*D. melanogaster*)	ey-GAL4-DBD	Lacin et al., 2019	RRID:BDSC 6294	
Genetic reagent (*D. melanogaster*)	y[1] w[*]; Mi{y[+mDint2]=MIC}Ets65A[MI05707]	BDSC	RRID:BDSC 40235	
Genetic reagent (*D. melanogaster*)	y[1] w[*]; TI{GFP[3xP3.cLa]=CRIMIC.TG4.2}sv[CR00370-TG4.2]	BDSC	RRID:BDSC 78901	

Genetic reagent (*D. melanogaster*)	y[1] w[*]; TI{GFP[3xP3.cLa]=CRIMIC.TG4.2}Sox21a[CR00451-TG4.2]/TM3 Sb[1] Ser[1]	BDSC	RRID:BDSC 83174	
Genetic reagent (*D. melanogaster*)	y[1] w[*] Mi{y[+mDint2]=MIC}bi[MI08152] lncRNA:CR32773[MI08152]	BDSC	RRID:BDSC 51220	
Genetic reagent (*D. melanogaster*)	y[1] w[*]; Mi{y[+mDint2]=MIC}ap[MI01996]/CyO	BDSC	RRID:BDSC 42297	
Genetic reagent (*D. melanogaster*)	y[1] w[*]; Mi{y[+mDint2]=MIC}inv[MI09433]	BDSC	RRID:BDSC 52163	
Genetic reagent (*D. melanogaster*)	y[1] w[*] Mi{y[+mDint2]=MIC}acj6[MI07818]	BDSC	RRID:BDSC 51212	
Genetic reagent (*D. melanogaster*)	y[1] w[*]; Mi{PT-GFSTF.2}Hmx[MI02025-GFSTF.2]/TM3, Sb[1] Ser[1]	BDSC	RRID:BDSC 59785	
Genetic reagent (*D. melanogaster*)	y[1] w[*]; Mi{y[+mDint2]=MIC}Hmx[MI02896]	BDSC	RRID:BDSC 36161	
Genetic reagent (*D. melanogaster*)	y[1] w[*]; Mi{y[+mDint2]=MIC}Ets65A[MI05707]	BDSC	RRID:BDSC 40235	
Genetic reagent (*D. melanogaster*)	y[1]; Mi{y[+mDint2]=MIC}toy[MI03240]	BDSC	RRID:BDSC 61701	
Genetic reagent (*D. melanogaster*)	P{Tub-dVP16AD.D}	BDSC	RRID:BDSC 60295	
Genetic reagent (*D. melanogaster*)	P{Tub-GAL4DBD.D}	BDSC	RRID:BDSC 60298	
Genetic reagent (*D. melanogaster*)	lim3-GAL4-DBD	Lacin et al., 2019	RRID:BDSC 82990	
Genetic reagent (*D. melanogaster*)	ChAT-p65.AD	Lacin lab		RMCE with RRID:BDSC37817
Genetic reagent (*D. melanogaster*)	y[*]w[*]/w[*];inv[MI09433.p65AD_1]/SM6a	generated in this study		RMCE with RRID:BDSC 52163
Genetic reagent (*D. melanogaster*)	ap-GAL4-DBD	generated in this study		RMCE with RRID:BDSC 42297
Genetic reagent (*D. melanogaster*)	ap-p65.AD	generated in this study		RMCE with RRID:BDSC 42297
Genetic reagent (*D. melanogaster*)	mab-21-GAL4-DBD	generated in this study		RMCE with RRID:BDSC 59220
Genetic reagent (*D. melanogaster*)	mab-21-p65.AD	generated in this study		RMCE with RRID:BDSC 59220

Genetic reagent (*D. melanogaster*)	toy-GAL4-DBD	generated in this study		RMCE with RRID:BDSC 61701
Genetic reagent (*D. melanogaster*)	toy-p65.AD	generated in this study		RMCE with RRID:BDSC 61701
Genetic reagent (*D. melanogaster*)	shaven-p65.AD	generated in this study		RMCE with RRID:BDSC 78901
Genetic reagent (*D. melanogaster*)	sox21a-GAL4-DBD	generated in this study		RMCE with RRID:BDSC 93174
Genetic reagent (*D. melanogaster*)	bi-GAL4-DBD	generated in this study		RMCE with RRID:BDSC 51220
Genetic reagent (*D. melanogaster*)	bi-p65.AD	generated in this study		RMCE with RRID:BDSC 51220
Genetic reagent (*D. melanogaster*)	CG4328-p65.AD	generated in this study		RMCE with RRID:BDSC 42307
Genetic reagent (*D. melanogaster*)	Ets65A-GAL4-DBD	generated in this study		RMCE with RRID:BDSC 56352
Genetic reagent (*D. melanogaster*)	Hmx-GAL4-DBD	generated in this study		RMCE with RRID:BDSC 36161
Genetic reagent (*D. melanogaster*)	dmrt99b-GAL4-DBD	generated in this study		RMCE with RRID:BDSC 92707
Genetic reagent (*D. melanogaster*)	dmrt99b-p65.AD	generated in this study		RMCE with RRID:BDSC 92707
Genetic reagent (*D. melanogaster*)	Dr-GAL4-DBD	generated in this study		RMCE with RRID:BDSC 59504
Genetic reagent (*D. melanogaster*)	exex-GAL4-DBD	generated in this study		RMCE with exex-p65AD[attP2FRT2]
Genetic reagent (*D. melanogaster*)	vg-GAL4-DBD	generated in this study		RMCE with vg-p65AD[attP2FRT2]
Genetic reagent (D. melanogaster)	sens2-p65.AD	generated in this study		RMCE with sens2-GAL4-DBD[attP2FRT
Genetic reagent (*D. melanogaster*)	Ets21C-GAL4-DBD	generated in this study		RMCE with Ets21C-p65.AD[attP2FRT2]

Genetic reagent (*D. melanogaster*)	eve-GAL4-DBD	generated in this study		RMCE with eve-p65.AD[attP2FRT2]
Genetic reagent (*D. melanogaster*)	exex-p65.AD[attP2FRT2]	generated in this study		CRISPR /Trojan (CRIMIC)
Genetic reagent (*D. melanogaster*)	exex-GAL4-DBD[attP2FRT2]	generated in this study		CRISPR /Trojan (CRIMIC)
Genetic reagent (*D. melanogaster*)	eve-p65.AD[attP2FRT2]	generated in this study		CRISPR /Trojan (CRIMIC)
Genetic reagent (*D. melanogaster*)	vg-p65.AD[attP2FRT2]	generated in this study		CRISPR /Trojan (CRIMIC)
Genetic reagent (*D. melanogaster*)	vg-GAL4-DBD[attP2FRT2]	generated in this study		CRISPR /Trojan (CRIMIC)
Genetic reagent (*D. melanogaster*)	H15-p65.AD[attP2FRT2]	generated in this study		CRISPR /Trojan (CRIMIC)
Genetic reagent (*D. melanogaster*)	scro-p65.AD[attP2FRT2]	generated in this study		CRISPR /Trojan (CRIMIC)
Genetic reagent (*D. melanogaster*)	scro-GAL4-DBD[attP2FRT2]	generated in this study		CRISPR /Trojan (CRIMIC)
Genetic reagent (*D. melanogaster*)	Ets21C-p65.AD[attP2FRT2]	generated in this study		CRISPR /Trojan (CRIMIC)
Genetic reagent (*D. melanogaster*)	Ets21C-GAL4-DBD[attP2FRT2]	generated in this study		CRISPR /Trojan (CRIMIC)
Genetic reagent (*D. melanogaster*)	eve-p65.AD[attP2FRT2]	generated in this study		CRISPR /Trojan (CRIMIC)
Genetic reagent (*D. melanogaster*)	Fer3-GAL4-DBD	generated in this study		CRISPR /In frame insertion (C terminus)
Genetic reagent (*D. melanogaster*)	ems-GAL4-DBD	generated in this study		CRISPR /In frame insertion (C terminus)
Genetic reagent (*D. melanogaster*)	HLH4C-GAL4-DBD	generated in this study		CRISPR /In frame insertion (2nd exon)
Genetic reagent (*D. melanogaster*)	w1118;; fkh-T2A-GAL4-DBD/TM6b	generated in this study		
Genetic reagent (*D. melanogaster*)	w*;; D-VP16/TM6b	generated in this study		
Genetic reagent (*D. melanogaster*)	pJFRC29-10XUAS-IVS-myr::GFP-p10 in attP40 or attP2	Rubin Lab		-
Genetic reagent (*D. melanogaster*)	pJFRC105-10XUAS-IVS-nlstdTomato in VK0003	Rubin Lab		-

Genetic reagent (*D. melanogater*)	pJFRC12-10XUAS-IVS-myr::GFP attp40 or attP2	Rubin Lab		
Genetic reagent (*D. melanogater*)	pJFRC28-10XUAS-IVS-GFP-p10 in attP2	Rubin Lab		
Chemical compound, drug	Paraformaldehyde	EMS	15713	
Chemical compound, drug	Vectashield	Vectorlabs	H-1000	
Chemical compound, drug	DPX	Electron Microscopy Sciences	50980370	
Chemical compound, drug	Gibson Assembly® Master Mix	New England Biolabs	E2621S	
Recombinant DNA reagent	pCFD4-U6:1_U6:3tandemgRNAs	Addgene	49411	
Recombinant DNA reagent	pBS-KS-attB2-SA(1)-T2A-Gal4-Hsp70	Addgene	62897	
Recombinant DNA reagent	pBS-KS-attB2-SA(1)-T2A-Gal4DBD-Hsp70	Addgene	62903	
Recombinant DNA reagent	pBS-KS-attB2-SA(1)-T2A-p65AD-Hsp70	Addgene	62914	
Recombinant DNA reagent	pBS-KS-attB2-SA(0)-T2A-Gal4-Hsp70	Addgene	62896	
Recombinant DNA reagent	pBS-KS-attB2-SA(0)-T2A-Gal4DBD-Hsp70	Addgene	62902	
Recombinant DNA reagent	pBS-KS-attB2-SA(0)-T2A-p65AD-Hsp70	Addgene	62912	
Recombinant DNA reagent	pBS-KS-attP2FRT2-SA(0)-T2A-p65AD-Hsp70	generated in this study		
Recombinant DNA reagent	pBS-KS-attP2FRT2-SA(1)-T2A-p65AD-Hsp70	generated in this study		
Recombinant DNA reagent	pBS-KS-attP2FRT2-SA(2)-T2A-p65AD-Hsp70	generated in this study		
Recombinant DNA reagent	pBS-KS-attP2FRT2-SA(0)-T2A-gal4DBD-Hsp70	generated in this study		
Recombinant DNA reagent	pBS-KS-attP2FRT2-SA(1)-T2A-gal4DBD-Hsp70	generated in this study		
Recombinant DNA reagent	pBS-KS-attP2FRT2-SA(2)-T2A-gal4DBD-Hsp70	generated in this study		
Recombinant DNA reagent	pCFD4-exex	generated in this study		
Recombinant DNA reagent	pCFD4-vg	generated in this study		
Recombinant DNA reagent	pCFD4-H15	generated in this study		
Recombinant DNA reagent	pUC57_Hb9	generated in this study		
Recombinant DNA reagent	pUC57_vg	generated in this study		
Recombinant DNA reagent	pUC57_H15	generated in this study		
Recombinant DNA reagent	pUC57_gw_OK2_Scro	generated in this study		

Recombinant DNA reagent	pUC57_gw_OK2_Ets21C	generated in this study		
Recombinant DNA reagent	pUC57_gw_OK2_eve	generated in this study		
Recombinant DNA reagent	pUC57_gw_OK2_Fer3	generated in this study		
Recombinant DNA reagent	pUC57_gw_OK2_ems	generated in this study		
Recombinant DNA reagent	pUC57_gw_OK2_HLH4C	generated in this study		

948

References:

1. Marin EC, Morris BJ, Stürner T, Champion AS, Krzeminski D, Badalamente G, et al. Systematic annotation of a complete adult maleDrosophilanerve cord connectome reveals principles of functional organisation. Elife.
2. Azevedo A, Lesser E, Phelps JS, Mark B, Elabbady L, Kuroda S, et al. Connectomic reconstruction of a female Drosophila ventral nerve cord. Nature. 2024;631(8020):360-8.
3. Li F, Lindsey JW, Marin EC, Otto N, Dreher M, Dempsey G, et al. The connectome of the adult Drosophila mushroom body provides insights into function. Elife. 2020;9.
4. Scheffer LK, Xu CS, Januszewski M, Lu Z, Takemura SY, Hayworth KJ, et al. A connectome and analysis of the adult Drosophila central brain. Elife. 2020;9.
5. Schlegel P, Yin Y, Bates AS, Dorkenwald S, Eichler K, Brooks P, et al. Whole-brain annotation and multi-connectome cell typing quantifies circuit stereotypy in Drosophila. bioRxiv. 2023.
6. Allen AM, Neville MC, Birtles S, Croset V, Treiber CD, Waddell S, et al. A single-cell transcriptomic atlas of the adult Drosophila ventral nerve cord. Elife. 2020;9.
7. Bates AS, Janssens J, Jefferis GS, Aerts S. Neuronal cell types in the fly: single-cell anatomy meets single-cell genomics. Curr Opin Neurobiol. 2019;56:125-34.
8. Özel MN, Simon F, Jafari S, Holguera I, Chen YC, Benhra N, et al. Neuronal diversity and convergence in a visual system developmental atlas. Nature. 2021;589(7840):88-95.
9. Yoo J, Dombrovski M, Mirshahidi P, Nern A, LoCascio SA, Zipursky SL, et al. Brain wiring determinants uncovered by integrating connectomes and transcriptomes. Curr Biol. 2023;33(18):3998-4005.e6.
10. Prokop A, Technau GM. The origin of postembryonic neuroblasts in the ventral nerve cord of Drosophila melanogaster. Development. 1991;111(1):79-88.
11. Truman JW. Metamorphosis of the central nervous system of Drosophila. J Neurobiol. 1990;21(7):1072-84.
12. Truman JW, Bate M. Spatial and temporal patterns of neurogenesis in the central nervous system of Drosophila melanogaster. Dev Biol. 1988;125(1):145-57.
13. Skeath JB, Doe CQ. Sanpodo and Notch act in opposition to Numb to distinguish sibling neuron fates in the Drosophila CNS. Development. 1998;125(10):1857-65.

14. Spana EP, Doe CQ. Numb antagonizes Notch signaling to specify sibling neuron cell fates. Neuron. 1996;17(1):21-6.

15. Truman JW, Moats W, Altman J, Marin EC, Williams DW. Role of Notch signaling in establishing the hemilineages of secondary neurons in Drosophila melanogaster. Development. 2010;137(1):53-61.

16. Ehrhardt E, Whitehead SC, Namiki S, Minegishi R, Siwanowicz I, Feng K, et al. Single-cell type analysis of wing premotor circuits in the ventral nerve cord of Drosophila melanogaster. bioRxiv. 2023.

17. Lesser E, Azevedo AW, Phelps JS, Elabbady L, Cook A, Syed DS, et al. Synaptic architecture of leg and wing premotor control networks in Drosophila. Nature. 2024;631(8020):369-77.

18. Agrawal S, Dickinson ES, Sustar A, Gurung P, Shepherd D, Truman JW, et al. Central processing of leg proprioception in Drosophila. Elife. 2020;9.

19. Harris RM, Pfeiffer BD, Rubin GM, Truman JW. Neuron hemilineages provide the functional ground plan for the Drosophila ventral nervous system. Elife. 2015;4.

20. Lacin H, Williamson WR, Card GM, Skeath JB, Truman JW. Unc-4 acts to promote neuronal identity and development of the take-off circuit in the Drosophila CNS. Elife. 2020;9.

21. Briscoe J, Pierani A, Jessell TM, Ericson J. A homeodomain protein code specifies progenitor cell identity and neuronal fate in the ventral neural tube. Cell. 2000;101(4):435-45.

22. Jessell TM. Neuronal specification in the spinal cord: inductive signals and transcriptional codes. Nat Rev Genet. 2000;1(1):20-9.

23. Lu DC, Niu T, Alaynick WA. Molecular and cellular development of spinal cord locomotor circuitry. Front Mol Neurosci. 2015;8:25.

24. Meissner GW, Vannan A, Jeter J, Close K, DePasquale GM, Dorman Z, et al. A split-GAL4 driver line resource for Drosophila CNS cell types. eLife Sciences Publications, Ltd; 2024.

25. Luan H, Diao F, Scott RL, White BH. The Drosophila Split Gal4 System for Neural Circuit Mapping. Front Neural Circuits. 2020;14:603397.

26. Pfeiffer BD, Ngo TT, Hibbard KL, Murphy C, Jenett A, Truman JW, et al. Refinement of tools for targeted gene expression in Drosophila. Genetics. 2010;186(2):735-55.

27. Lacin H, Zhu Y, Wilson BA, Skeath JB. Transcription factor expression uniquely identifies most postembryonic neuronal lineages in the Drosophila thoracic central nervous system. Development. 2014;141(5):1011-21.

28. Lacin H, Chen HM, Long X, Singer RH, Lee T, Truman JW. Neurotransmitter identity is acquired in a lineage-restricted manner in the Drosophila CNS. Elife. 2019;8.

29. Lacin H, Truman JW. Lineage mapping identifies molecular and architectural similarities between the larval and adult Drosophila central nervous system. Elife. 2016;5:e13399.

30. Lacin H, Zhu Y, DiPaola JT, Wilson BA, Zhu Y, Skeath JB. A genetic screen in Drosophila uncovers a role for senseless-2 in surface glia in the peripheral nervous system to regulate CNS morphology. G3 (Bethesda). 2024;14(9).

31. Chen YD, Chen YC, Rajesh R, Shoji N, Jacy M, Lacin H, et al. Using single-cell RNA sequencing to generate predictive cell-type-specific split-GAL4 reagents throughout development. Proc Natl Acad Sci U S A. 2023;120(32):e2307451120.

32. Diao F, Ironfield H, Luan H, Diao F, Shropshire WC, Ewer J, et al. Plug-and-play genetic access to drosophila cell types using exchangeable exon cassettes. Cell Rep. 2015;10(8):1410-21.

33. Luan H, Peabody NC, Vinson CR, White BH. Refined spatial manipulation of neuronal function by combinatorial restriction of transgene expression. Neuron. 2006;52(3):425-36.

34. Lacin H, Zhu Y, Wilson BA, Skeath JB. dbx mediates neuronal specification and differentiation through cross-repressive, lineage-specific interactions with eve and hb9. Development. 2009;136(19):3257-66.

35. Kuert PA, Hartenstein V, Bello BC, Lovick JK, Reichert H. Neuroblast lineage identification and lineage-specific Hox gene action during postembryonic development of the subesophageal ganglion in the Drosophila central brain. Dev Biol. 2014;390(2):102-15.

36. Shepherd D, Sahota V, Court R, Williams DW, Truman JW. Developmental organization of central neurons in the adult Drosophila ventral nervous system. J Comp Neurol. 2019;527(15):2573-98.

37. Lee T, Luo L. Mosaic Analysis with a Repressible Cell Marker for Studies of Gene Function in Neuronal Morphogenesis. Neuron. 1999;22(3):451-61.

38. Nagarkar-Jaiswal S, Lee PT, Campbell ME, Chen K, Anguiano-Zarate S, Gutierrez MC, et al. A library of MiMICs allows tagging of genes and reversible, spatial and temporal knockdown of proteins in Drosophila. Elife. 2015;4.

39. Li SA, Li HG, Shoji N, Desplan C, Chen Y-CD. Protocol for replacing coding intronic MiMIC and CRIMIC lines with T2A-split-GAL4 lines in Drosophila using genetic crosses. STAR Protocols. 2023;4(4):102706.

40. Chen N, Zhang Y, Rivera-Rodriguez EJ, Yu AD, Hobin M, Rosbash M, et al. Widespread posttranscriptional regulation of cotransmission. Sci Adv. 2023;9(22):eadg9836.

41. Klapoetke NC, Murata Y, Kim SS, Pulver SR, Birdsey-Benson A, Cho YK, et al. Independent optical excitation of distinct neural populations. Nat Methods. 2014;11(3):338-46.

42. Simpson JH. Rationally subdividing the fly nervous system with versatile expression reagents. J Neurogenet. 2016;30(3-4):185-94.

43. Namiki S, Dickinson MH, Wong AM, Korff W, Card GM. The functional organization of descending sensory-motor pathways in Drosophila. Elife. 2018;7.

44. Namiki S, Ros IG, Morrow C, Rowell WJ, Card GM, Korff W, et al. A population of descending neurons that regulates the flight motor of Drosophila. Curr Biol. 2022;32(5):1189-96.e6.

45. Zabala FA, Card GM, Fontaine EI, Dickinson MH, Murray RM. Flight dynamics and control of evasive maneuvers: the fruit fly's takeoff. IEEE Trans Biomed Eng. 2009;56(9):2295-8.

46. Card G, Dickinson M. Performance trade-offs in the flight initiation of Drosophila. J Exp Biol. 2008;211(Pt 3):341-53.

47. Cheong HSJ, Eichler K, Stürner T, Asinof SK, Champion AS, Marin EC, et al. Transforming descending input into behavior: The organization of premotor circuits in the Drosophila Male Adult Nerve Cord connectome. bioRxiv. 2024:2023.06.07.543976.

48. Plaza SM, Clements J, Dolafi T, Umayam L, Neubarth NN, Scheffer LK, et al. neuPrint: An open access tool for EM connectomics. Front Neuroinform. 2022;16:896292.

49. Takemura S-y, Hayworth KJ, Huang GB, Januszewski M, Lu Z, Marin EC, et al. A Connectome of the MaleDrosophilaVentral Nerve Cord.

50. Doe CQ, Goodman CS. Early events in insect neurogenesis. II. The role of cell interactions and cell lineage in the determination of neuronal precursor cells. Dev Biol. 1985;111(1):206-19.

51. Hartenstein V, Omoto JJ, Ngo KT, Wong D, Kuert PA, Reichert H, et al. Structure and development of the subesophageal zone of the Drosophila brain. I. Segmental architecture, compartmentalization, and lineage anatomy. J Comp Neurol. 2018;526(1):6-32.

52. Li HH, Kroll JR, Lennox SM, Ogundeyi O, Jeter J, Depasquale G, et al. A GAL4 driver resource for developmental and behavioral studies on the larval CNS of Drosophila. Cell Rep. 2014;8(3):897-908.

53. Xie Q, Brbic M, Horns F, Kolluru SS, Jones RC, Li J, et al. Temporal evolution of single-cell transcriptomes of Drosophila olfactory projection neurons. Elife. 2021;10.

54. Xie Q, Wu B, Li J, Xu C, Li H, Luginbuhl DJ, et al. Transsynaptic Fish-lips signaling prevents misconnections between nonsynaptic partner olfactory neurons. Proc Natl Acad Sci U S A. 2019;116(32):16068-73.

55. Polstein LR, Gersbach CA. A light-inducible CRISPR-Cas9 system for control of endogenous gene activation. Nat Chem Biol. 2015;11(3):198-200.

56. Mohammad F, Stewart JC, Ott S, Chlebikova K, Chua JY, Koh TW, et al. Optogenetic inhibition of behavior with anion channelrhodopsins. Nat Methods. 2017;14(3):271-4.

57. Akin O, Bajar BT, Keles MF, Frye MA, Zipursky SL. Cell-type-Specific Patterned Stimulus-Independent Neuronal Activity in the Drosophila Visual System during Synapse Formation. Neuron. 2019;101(5):894-904.e5.

58. Bajar BT, Phi NT, Isaacman-Beck J, Reichl J, Randhawa H, Akin O. A discrete neuronal population coordinates brain-wide developmental activity. Nature. 2022;602(7898):639-46.

59. Liu LY, Long X, Yang CP, Miyares RL, Sugino K, Singer RH, et al. Mamo decodes hierarchical temporal gradients into terminal neuronal fate. Elife. 2019;8.

60. Maurange C, Cheng L Fau - Gould AP, Gould AP. Temporal transcription factors and their targets schedule the end of neural proliferation in Drosophila. (1097-4172 (Electronic)).

61. Zhu S, Lin S, Kao CF, Awasaki T, Chiang AS, Lee T. Gradients of the Drosophila Chinmo BTB-zinc finger protein govern neuronal temporal identity. Cell. 2006;127(2):409-22.

62. Zhou B, Williams DW, Altman J, Riddiford LM, Truman JW. Temporal patterns of broad isoform expression during the development of neuronal lineages in Drosophila. Neural Dev. 2009;4:39.

63. Nern A, Pfeiffer BD, Rubin GM. Optimized tools for multicolor stochastic labeling reveal diverse stereotyped cell arrangements in the fly visual system. Proc Natl Acad Sci U S A. 2015;112(22):E2967-76.

64. Gratz SJ, Ukken FP, Rubinstein CD, Thiede G, Donohue LK, Cummings AM, et al. Highly specific and efficient CRISPR/Cas9-catalyzed homology-directed repair in Drosophila. Genetics. 2014;196(4):961-71.

65. Port F, Chen HM, Lee T, Bullock SL. Optimized CRISPR/Cas tools for efficient germline and somatic genome engineering in Drosophila. Proc Natl Acad Sci U S A. 2014;111(29):E2967-76.

66. Kanca O, Zirin J, Garcia-Marques J, Knight SM, Yang-Zhou D, Amador G, et al. An efficient CRISPR-based strategy to insert small and large fragments of DNA using short homology arms. eLife. 2019;8:e51539.

67. Kanca O, Zirin J, Hu Y, Tepe B, Dutta D, Lin WW, et al. An expanded toolkit for Drosophila gene tagging using synthesized homology donor constructs for CRISPR-mediated homologous recombination. Elife. 2022;11.

68. Kondo S, Ueda R. Highly improved gene targeting by germline-specific Cas9 expression in Drosophila. Genetics. 2013;195(3):715-21.

69. Truman JW, Schuppe H, Shepherd D, Williams DW. Developmental architecture of adult-specific lineages in the ventral CNS of Drosophila. Development. 2004;131(20):5167-84.

FIGURE 1

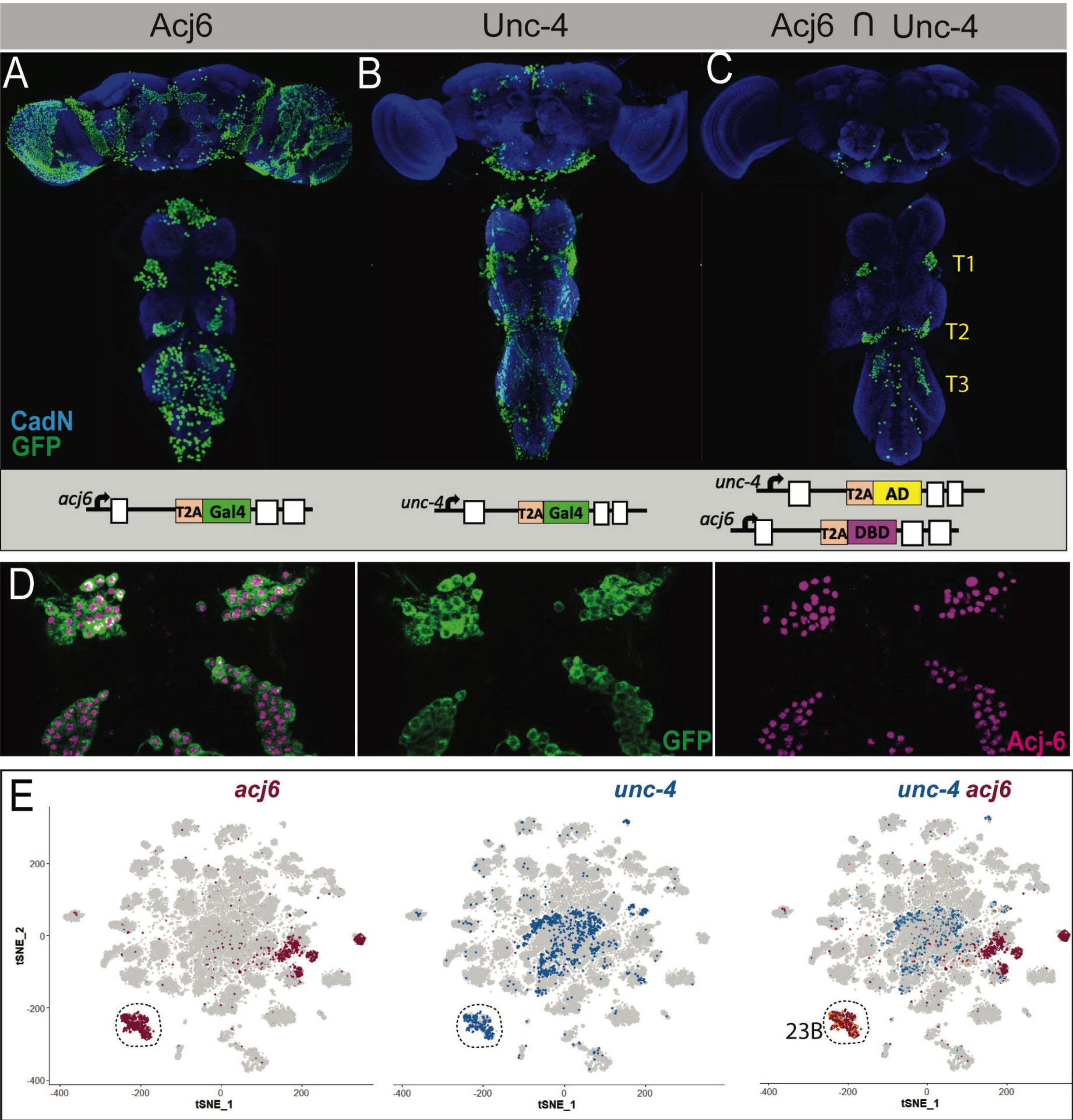
Acj6
Unc-4
Acj6 ∩ Unc-4
A
B
C
T1
T2
T3
CadN
GFP
acj6
T2A
Gal4
unc-4
T2A
Gal4
unc-4
T2A
AD
acj6
T2A
DBD
D
GFP
Acj-6
E
acj6
unc-4
unc-4 acj6
tSNE_2
tSNE_1
23B

FIGURE 1-SUPP1

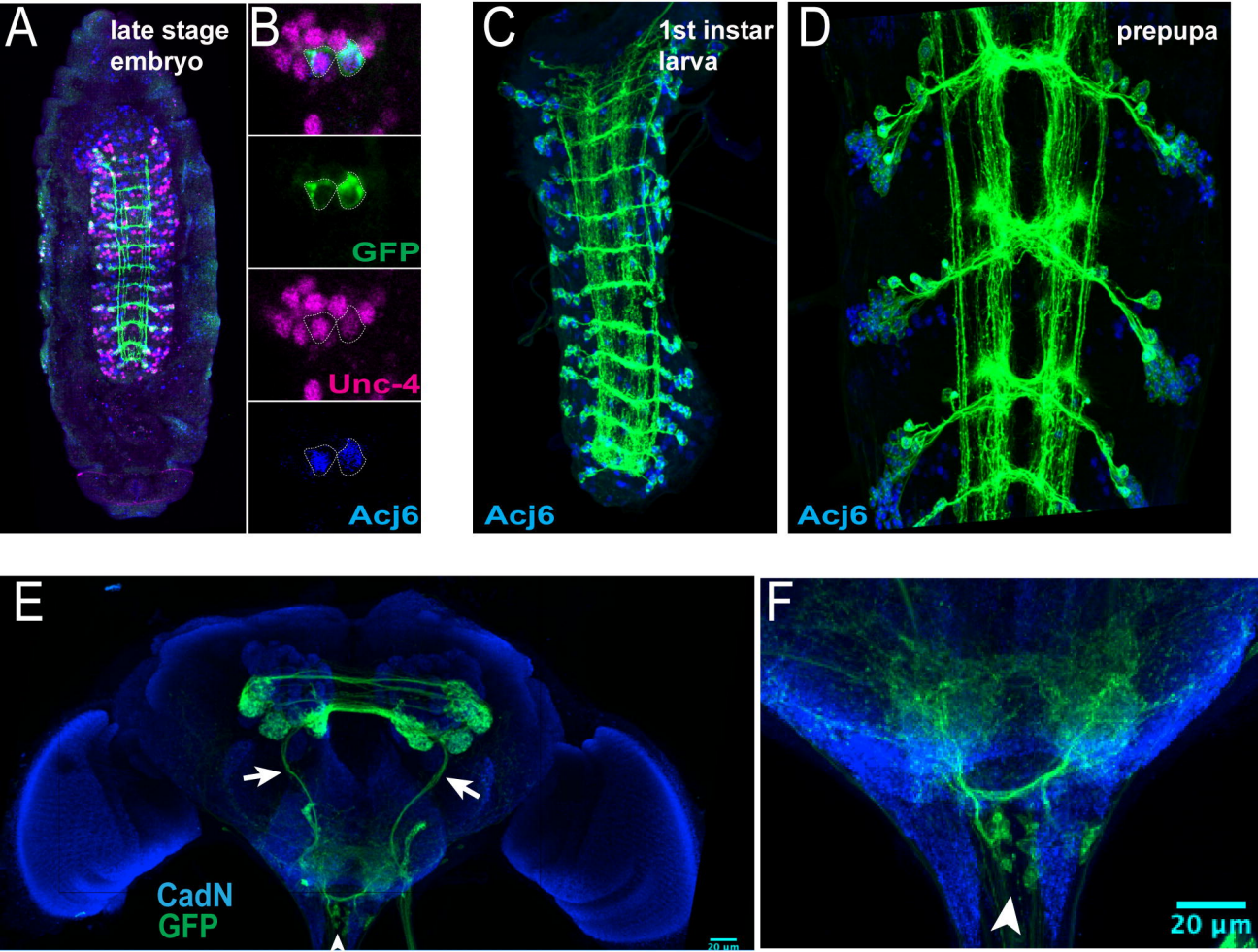

FIGURE 2

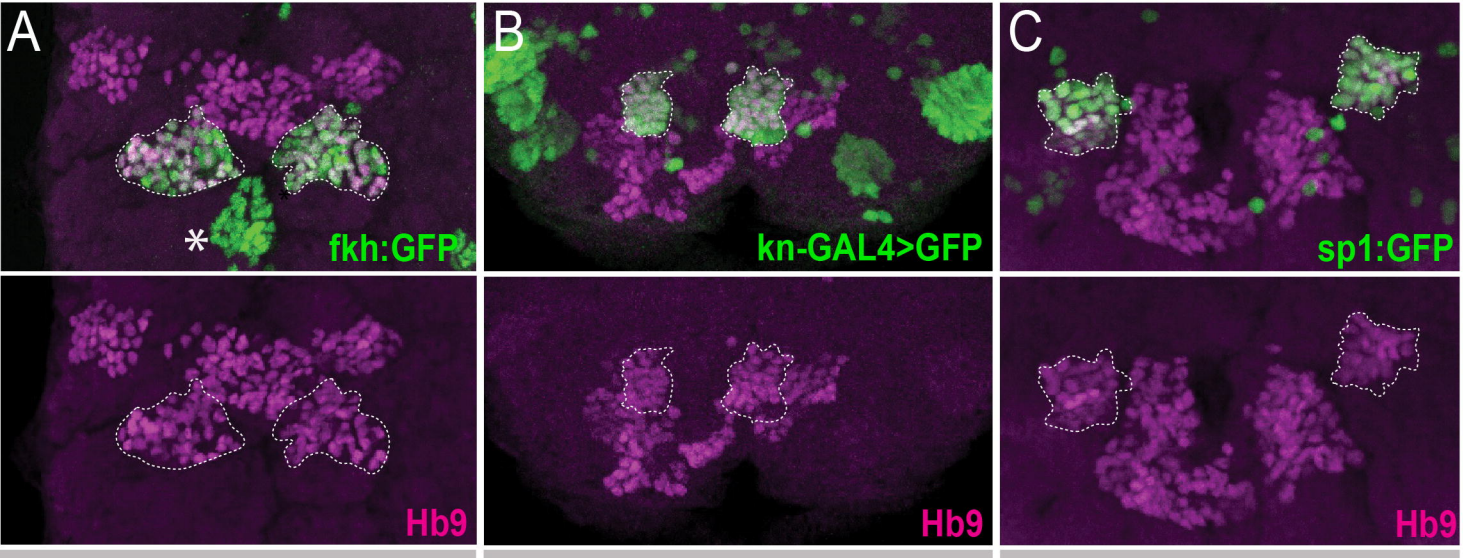

4B: clusters 0, 100 | **10B**: clusters 39, 68,91 | **16B**: clusters 5, 46

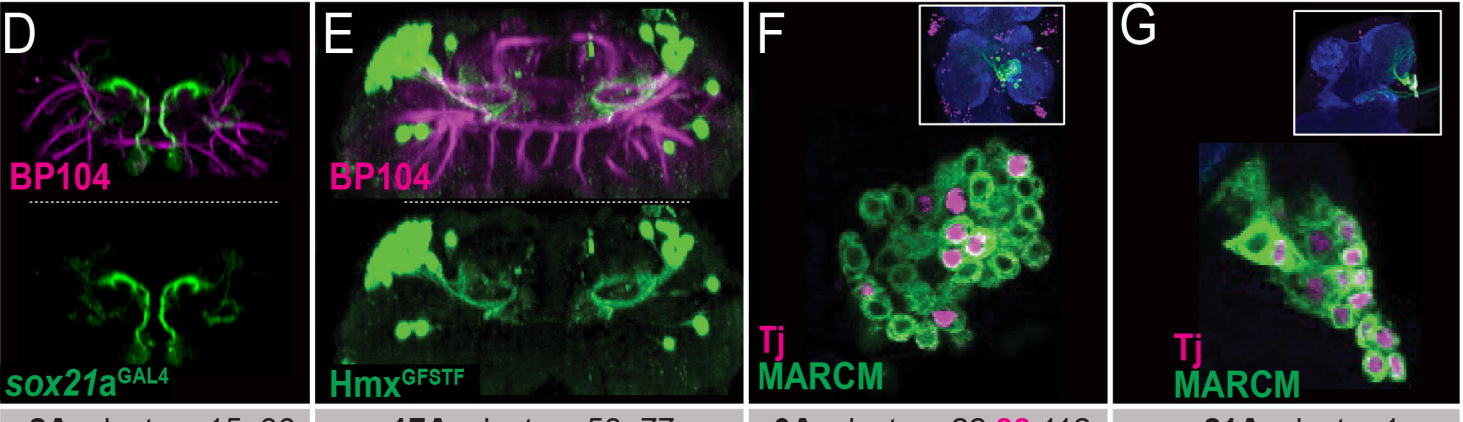

2A: clusters 15, 86 | **17A**: clusters 58 ,77 | **0A**: clusters 22,88,112 | **21A**: cluster 1

FIGURE 3

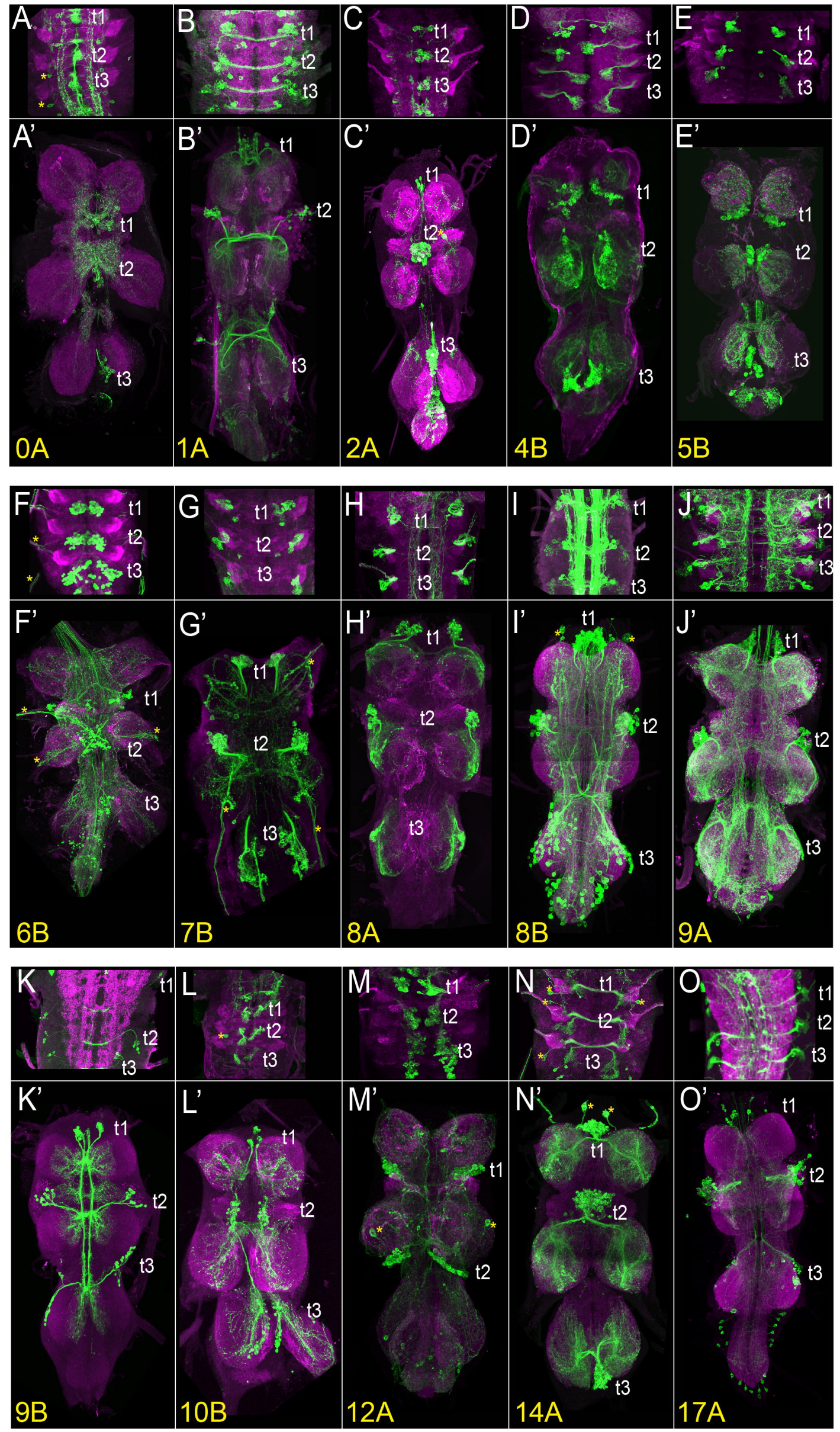
A
t1
t2
t3
B
t1
t2
t3
C
t1
t2
t3
D
t1
t2
t3
E
t1
t2
t3
A'
t1
t2
t3
0A
B'
t1
t2
t3
1A
C'
t1
t2
t3
2A
D'
t1
t2
t3
4B
E'
t1
t2
t3
5B
F
t1
t2
t3
G
t1
t2
t3
H
t1
t2
t3
I
t1
t2
t3
J
t1
t2
t3
F'
t1
t2
t3
6B
G'
t1
t2
t3
7B
H'
t1
t2
t3
8A
I'
t1
t2
t3
8B
J'
t1
t2
t3
9A
K
t1
t2
t3
L
t1
t2
t3
M
t1
t2
t3
N
t1
t2
t3
O
t1
t2
t3
K'
t1
t2
t3
9B
L'
t1
t2
t3
10B
M'
t1
t2
12A
N'
t1
t2
t3
14A
O'
t1
t2
t3
17A

FIGURE 3-SUPP1

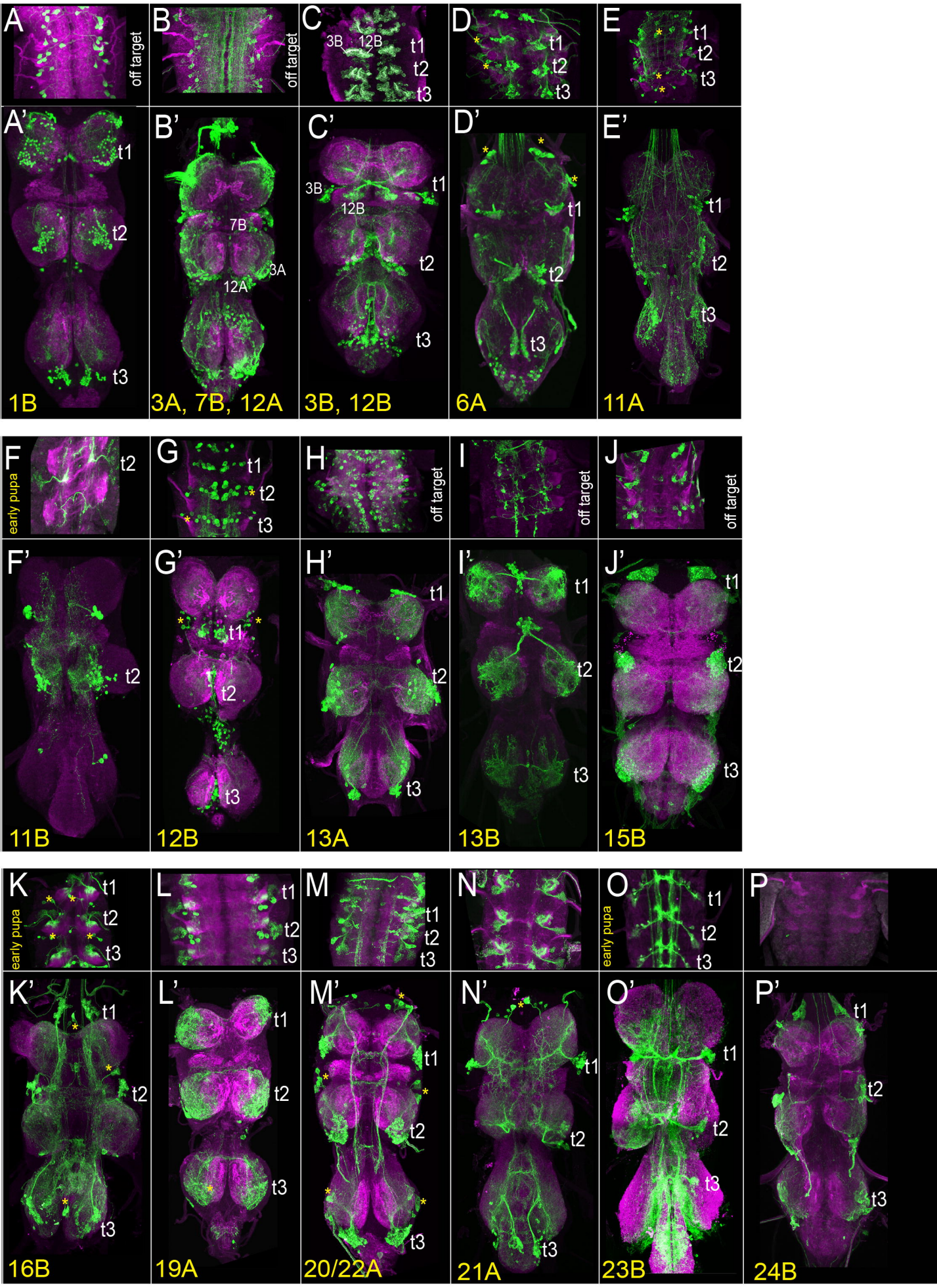

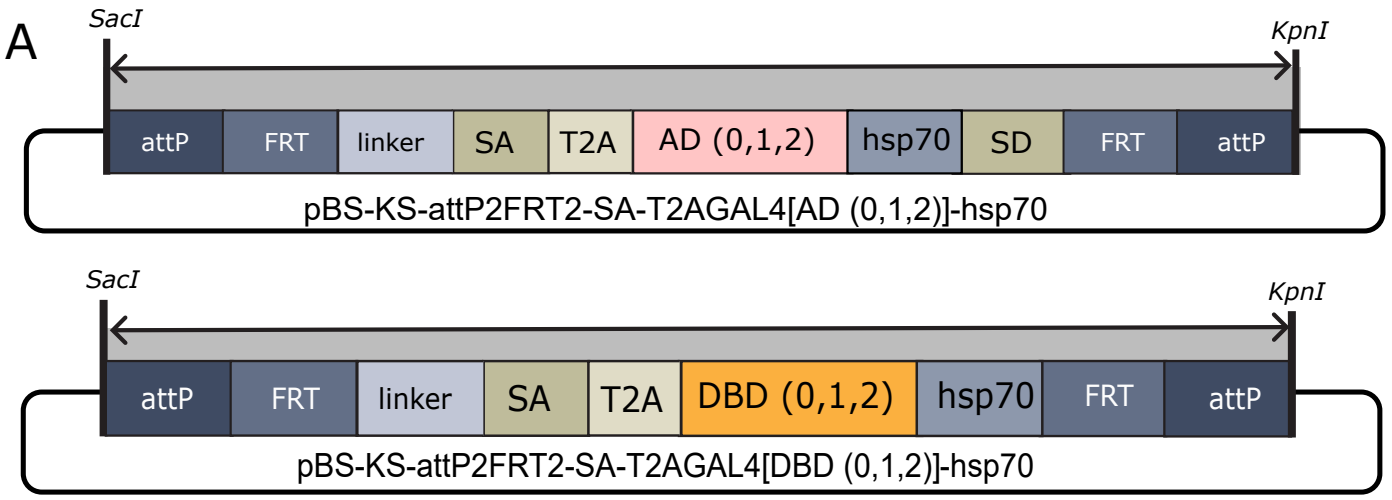
A
SacI
KpnI
attP
FRT
linker
SA
T2A
AD (0,1,2)
hsp70
SD
FRT
attP
pBS-KS-attP2FRT2-SA-T2AGAL4[AD (0,1,2)]-hsp70

SacI
KpnI
attP
FRT
linker
SA
T2A
DBD (0,1,2)
hsp70
FRT
attP
pBS-KS-attP2FRT2-SA-T2AGAL4[DBD (0,1,2)]-hsp70

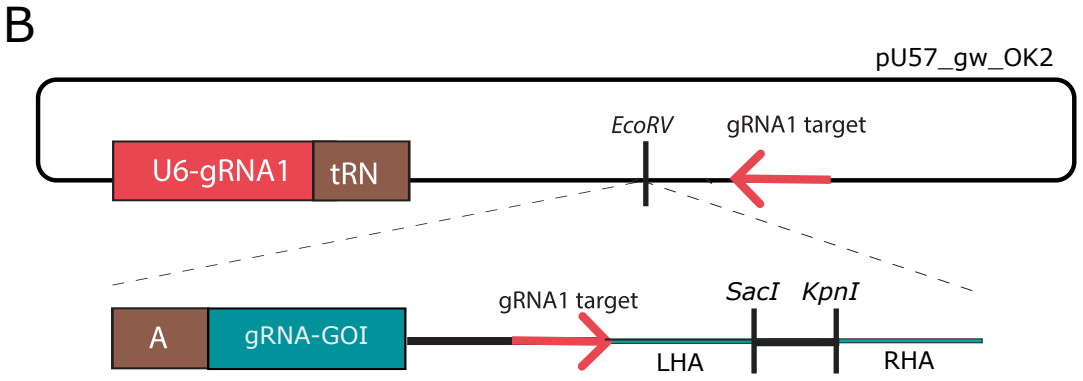
B
pU57_gw_OK2
U6-gRNA1
tRN
EcoRV
gRNA1 target
A
gRNA-GOI
gRNA1 target
SacI
KpnI
LHA
RHA

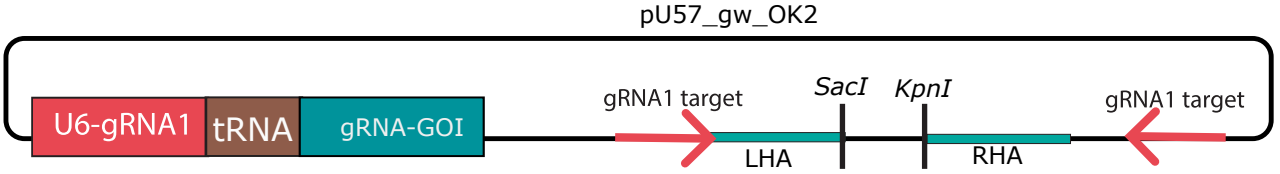
pU57_gw_OK2
U6-gRNA1
tRNA
gRNA-GOI
gRNA1 target
SacI
KpnI
gRNA1 target
LHA
RHA

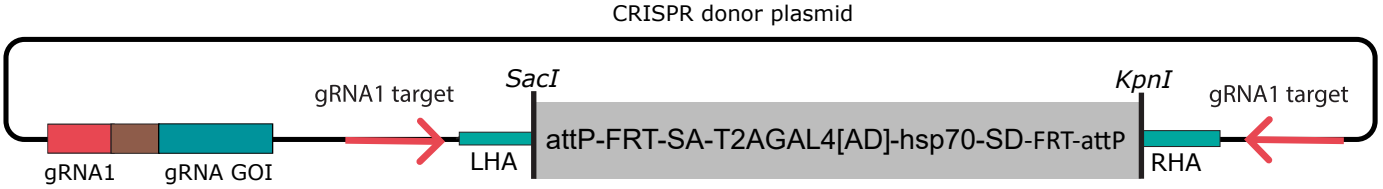
CRISPR donor plasmid
gRNA1 target
SacI
KpnI
gRNA1 target
gRNA1
gRNA GOI
LHA
attP-FRT-SA-T2AGAL4[AD]-hsp70-SD-FRT-attP
RHA

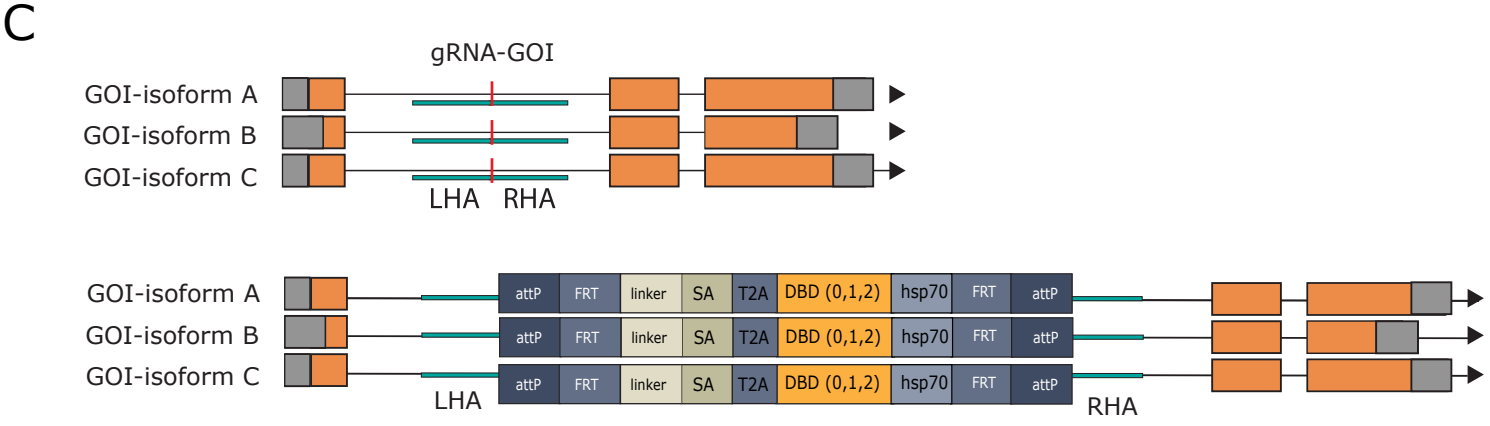
C
gRNA-GOI
GOI-isoform A
GOI-isoform B
GOI-isoform C
LHA
RHA
GOI-isoform A
GOI-isoform B
GOI-isoform C
attP
FRT
linker
SA
T2A
DBD (0,1,2)
hsp70
FRT
attP
LHA
RHA

FIGURE 3-SUPP3

A

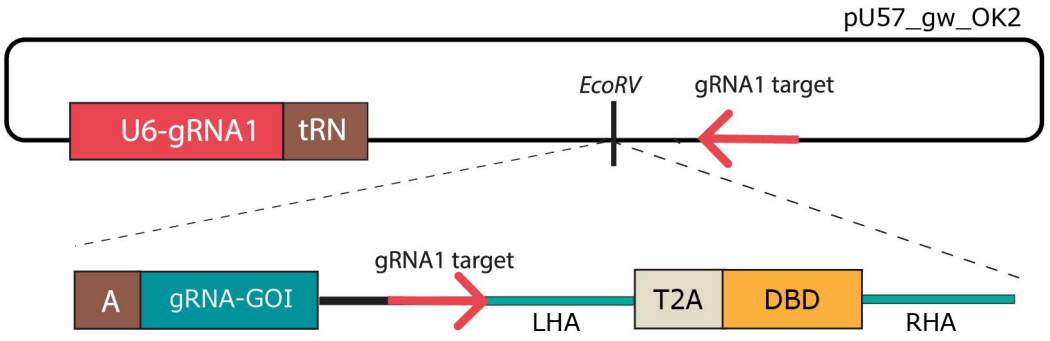

B

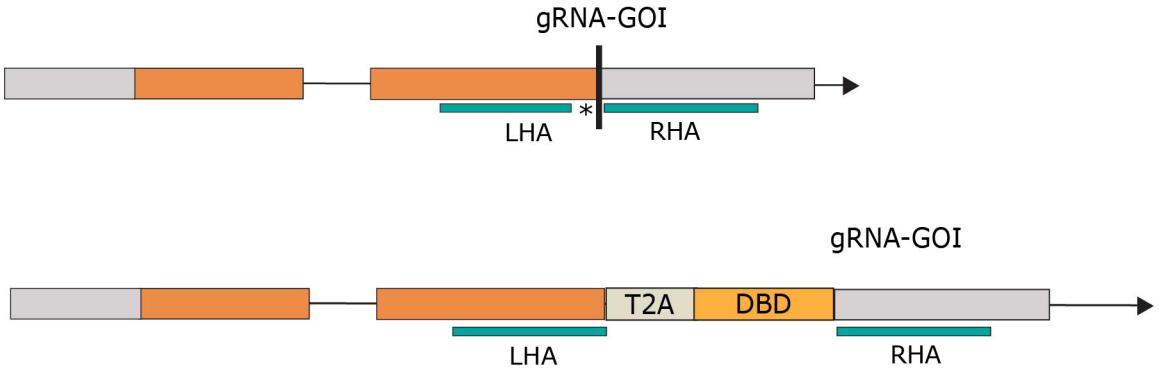

FIGURE 4

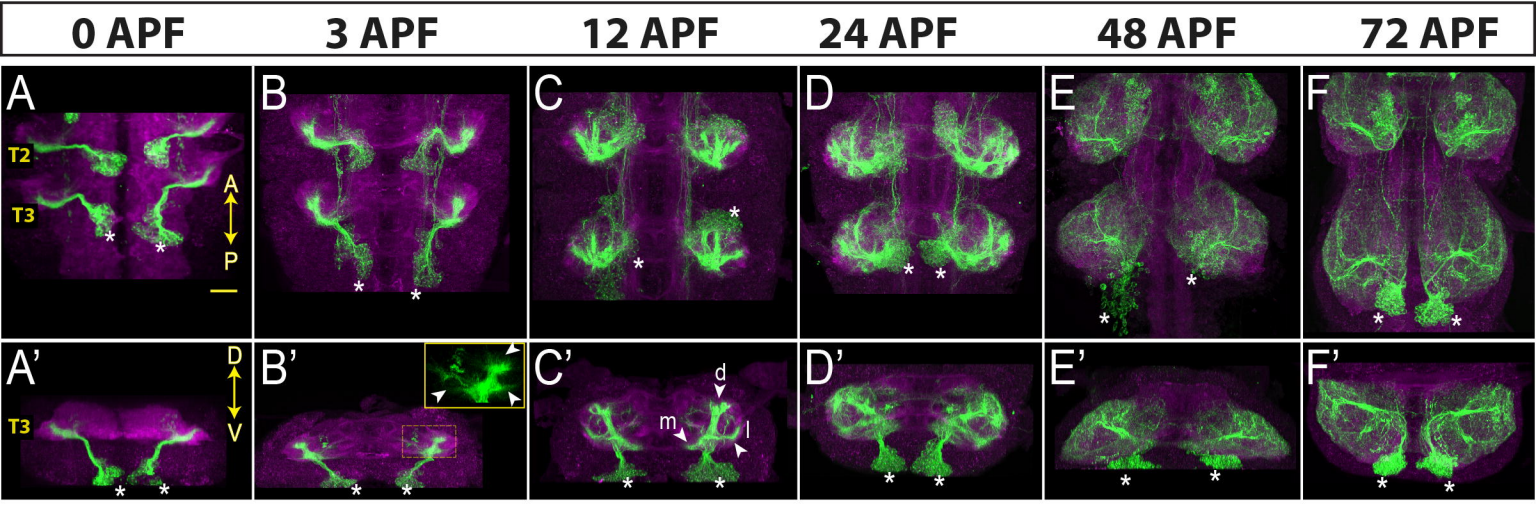
0 APF
3 APF
12 APF
24 APF
48 APF
72 APF
A
B
C
D
E
F
T2
T3
A
P
A'
B'
C'
D'
E'
F'
D
V
d
m
l

FIGURE 5

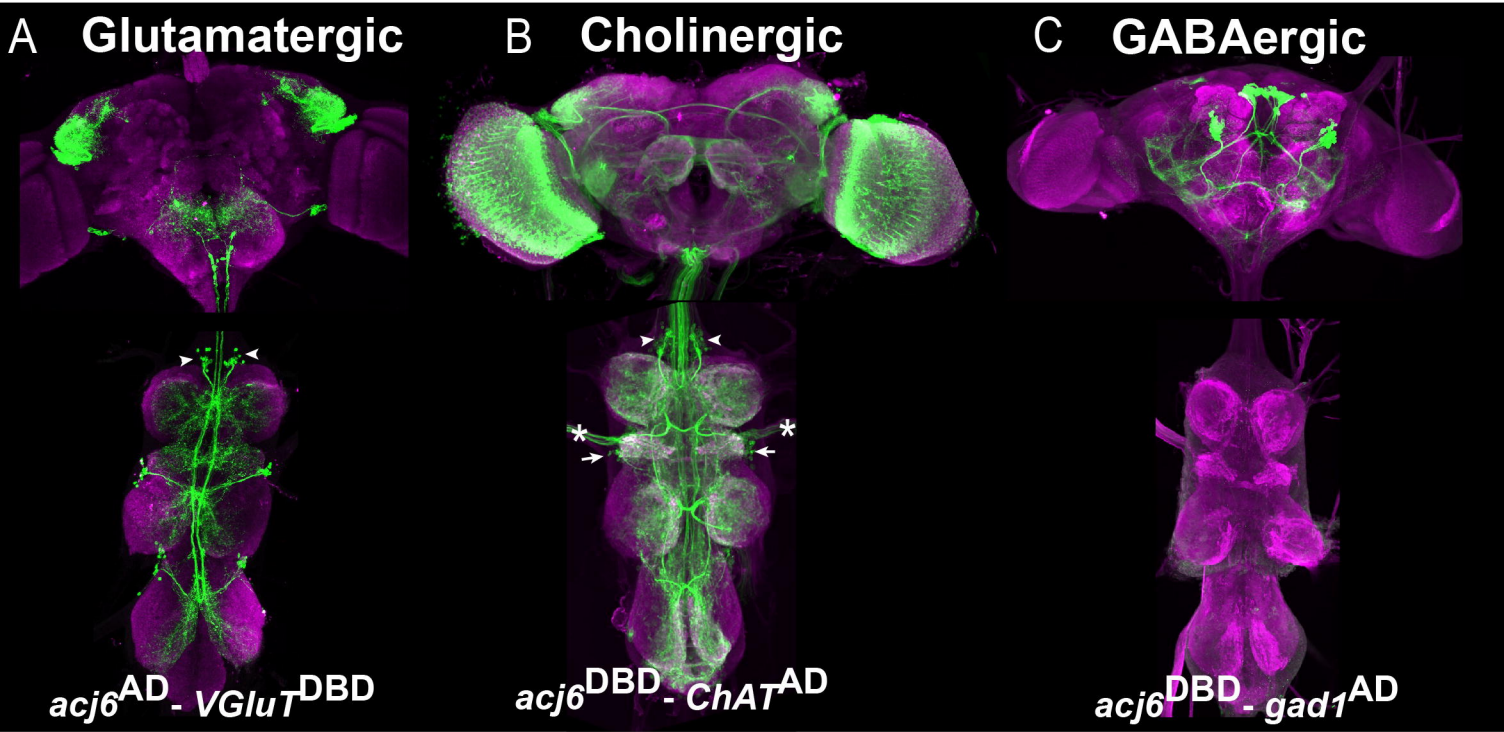
A Glutamatergic
B Cholinergic
C GABAergic
acj6AD - VGluTDBD
acj6DBD - ChATAD
acj6DBD - gad1AD

FIGURE 6

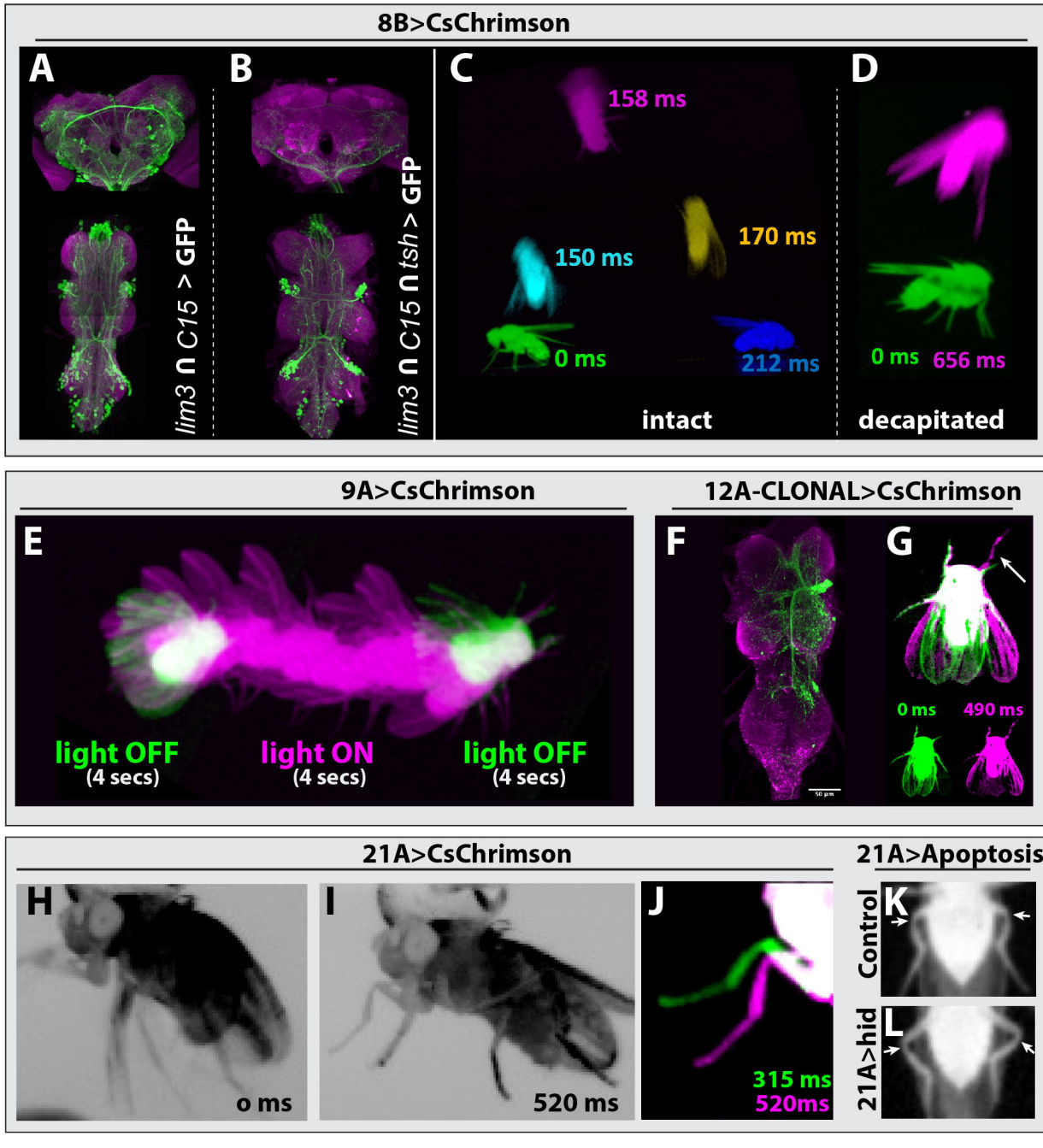
8B>CsChrimson
A
B
C
D
lim3 ∩ C15 > GFP
lim3 ∩ C15 ∩ tsh > GFP
158 ms
170 ms
150 ms
0 ms
212 ms
intact
0 ms
656 ms
decapitated
9A>CsChrimson
12A-CLONAL>CsChrimson
E
F
G
light OFF
(4 secs)
light ON
(4 secs)
light OFF
(4 secs)
0 ms
490 ms
21A>CsChrimson
21A>Apoptosis
H
I
J
K
L
Control
21A>hid
o ms
520 ms
315 ms
520ms
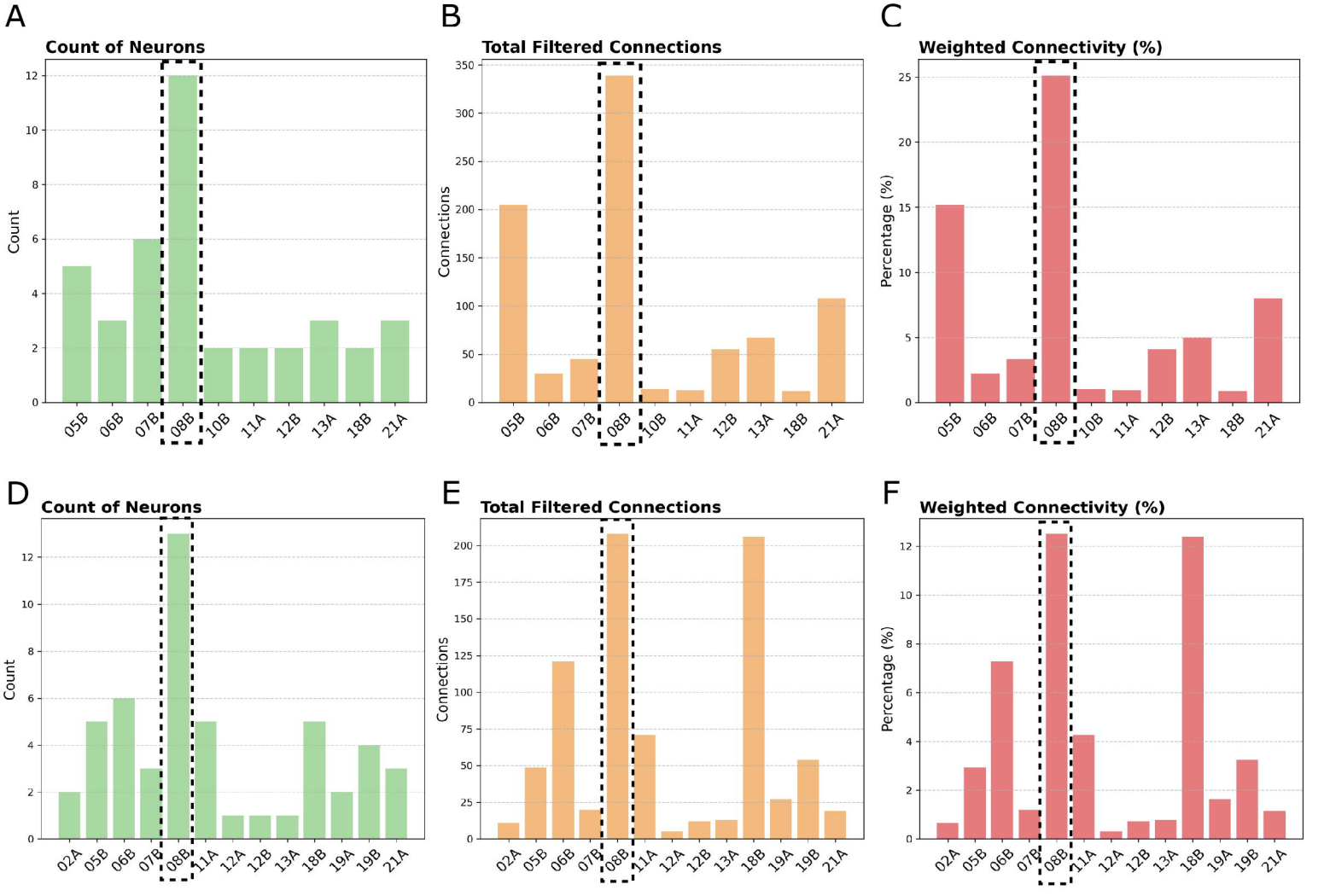
FIGURE 6-SUPP1